Bulletin of the Seismological Society of America. Vol. 66, No. 1, pp. 189–219. February 1976.

PRELIMINARY ANALYSIS OF THE PEAKS OF STRONG EARTHQUAKE GROUND MOTION—DEPENDENCE OF PEAKS ON EARTHQUAKE MAGNITUDE, EPICENTRAL DISTANCE, AND RECORDING SITE CONDITIONS

By M. D. Trifunac

ABSTRACT

Analyses of peak amplitudes of strong earthquake ground motion have been carried out with the emphasis on their dependence on earthquake magnitude, epicentral distance, and geological conditions at the recording site. Approximate empirical scaling functions have been developed which, for a selected confidence level, yield an estimate of an upper bound of peak accelerations, velocities, and displacements. The parameters in these scaling functions have been computed by least-squares fitting of the recorded data on peak amplitudes which are now available for a range of epicentral distances between about 20 and 200 km and are representative for the period from 1933 to 1971 in the Western United States.

The possibility of extrapolating the derived scaling laws to small epicentral distances where no strong-motion data are currently available has been tested by comparing predicted peak amplitudes with related parameters at the earthquake source. These source parameters (average dislocation and stress drop) can be derived from other independent studies and do not contradict the inferences presented in this paper. It has been found that for an approximate 90 per cent confidence level the presently available data suggest that peak accelerations, velocities, and displacements at the fault and for the frequency band between 0.07 and 25 Hz probably do not exceed about 3 to 5 g, 400 to 700 cm/sec, and 200 to 400 cm, respectively.

The logarithms of the peaks of strong ground motion seem to depend in a linear manner on earthquake magnitude only for small shocks. For large magnitudes this dependence disappears gradually and maximum amplitudes may be achieved for $M \approx 7.5$. The influence of geological conditions at the recording site appears to be insignificant for peak accelerations but becomes progressively more important for peaks of strong-motion velocity and displacement.

Introduction

Since the early 1940's, numerous empirical scaling functions have been proposed and developed for prediction of peak ground acceleration as a function of earthquake magnitude and epicentral distance. Some other pertinent parameters which can be related to the characteristics of the recording sites have also been considered by several authors (Gutenberg and Richter, 1942; Newmann, 1954; Gutenberg and Richter, 1956; Blume, 1965; Housner, 1965; Kanai, 1966; Milne and Davenport, 1969; Esteva, 1970; Cloud and Perez, 1971; Donovan, 1972; Page *et al.*, 1972; Schnabel and Seed, 1973; Boore, 1973; Dietrich, 1973; Katayama, 1974). In our recent paper (Trifunac and Brady, 1975b) most of these scaling functions were reviewed and compared with the trends indicated by the strong-motion data now available for the Western United States. In the same paper it was shown that (a) peaks of strong ground motion do not grow linearly with magnitude, which

is in agreement with some previous investigations, and (b) that the soil conditions at a recording station have significant effect only for peak ground displacement and only minor to insignificant effect on peak accelerations and peak velocities. Finally, the new scaling functions which give the expected values and standard deviations for peaks of strong ground motion were presented.

The purpose of this paper is to extend this work by attaching approximate confidence levels to predicted peak amplitudes and to examine whether it is possible to develop a rational physical basis for the extrapolations of currently available results back to the earthquake source. It is felt that the computation of such approximate confidence levels for predicted peaks of strong ground motion may be useful in earthquake engineering applications, since it leads to more accurate and better defined procedures for scaling strong-motion amplitudes when the acceptable risk of exceeding a given level is known or is specified. Furthermore, the characterization of strong earthquake ground motion by the mean and standard deviation only of its peak amplitudes may not be adequate for some applications, since the distribution of measured amplitudes is not accurately known.

It has been found (Trifunac and Brady, 1975b) that the empirical law of the attenuation with distance (Richter, 1958), which is used for calculations of local earthquake magnitude, describes approximately the attenuation with distance of peak acceleration, velocity, and displacement data, but the adequacy of this approach for epicentral distances less than about 20 km has not been established. One of the main objectives in this paper is, therefore, to examine this problem in some detail. This can be done by comparing the predicted average dislocations and stress drops from the analysis of strong-motion data, which is carried out in this paper, with the independent estimates of these quantities derived from three detailed source mechanism studies which dealt with the corresponding geographical area (Trifunac, 1972a, 1972b; Thatcher and Hanks, 1973).

Finally, it should be noted here that the aim of this paper is to present the author's most recent assessment of what the actual recorded amplitudes of strong earthquake ground motion might be in the near-field. Although an effort is made in this work to test these estimates of predicted peak levels by comparing the results with independent calculations which are based on an approximate source mechanism theory, it must be remembered that the final test of the preliminary results we present in this paper can only come from future records of strong ground motion. While our present calculations may prove useful in earthquake engineering applications which require an estimate of actual strong-motion amplitudes, it should be emphasized that the strong-motion amplitudes discussed in this paper do not represent the design amplitudes for direct use in routine earthquake engineering calculations.

Strong-Motion Data

The amplitudes of peak acceleration, velocity, and displacement which are used in this study have been extracted from the Volume II tapes (Trifunac and Lee, 1973) which contain corrected accelerograms (Trifunac, 1971, 1972c) and integrated velocity and displacement curves (Hudson *et al.*, 1971). These data result from a strong-motion recording program in the Western United States and have been processed for the period beginning in 1933 and ending in 1971. The data consist of 187 accelerograph records (373 horizontal and 187 vertical components) which were obtained at "free-field" stations or in the basement floors of buildings. These data result from 57 earthquakes whose magnitudes range from 3.0 to 7.7. Of 187 records 6 or 3 per cent correspond to the magnitude range 4.0–4.9, 41 or 22 per cent to 5.0–5.9, 130 or 71 per cent to 6.0–6.9 and 7 or 3 per cent to the magnitude range 7.0–7.9. Sixty-three per cent of the data have been

recorded on alluvium sites (identified by $s = 0$ in this paper), 23 per cent on "intermediate" sites (identified by $s = 1$), and only 8 per cent on basement rock sites (identified by $s = 2$). Geological descriptions of these sites and the method employed to arrive at the final site classification used in this and our previous papers have been presented by Trifunac and Brady (1975a) and will not be repeated here.

Figures 1, 2, and 3 present the vertical and horizontal peaks of strong-motion data plotted versus epicentral distance in kilometers. Each peak is identified by its site classification symbol, "0", "1", or "2", and by the corresponding earthquake magnitude. Continuous curves in these figures represent predicted peak amplitudes for selected earthquake magnitudes equal to 4.5, 5.5, and 6.5. for the three site classifications and for a 90 per cent confidence level. The method for calculating these amplitudes will be discussed later in this paper.

Proposed Scaling for Peaks of Strong Ground Motion

It was recently suggested that the peaks of strong ground motion might be scaled by using the following expression

$$\log_{10}\begin{Bmatrix} a_{\max} \\ v_{\max} \\ d_{\max} \end{Bmatrix} = M + \log_{10} A_0(R) - \log_{10}\begin{Bmatrix} a_0(M) \\ v_0(M) \\ d_0(M) \end{Bmatrix} \tag{1}$$

(Trifunac and Brady, 1975b). In (1) $a_{\max}$, $v_{\max}$, and $d_{\max}$ represent peak acceleration, peak velocity, and peak displacement, respectively; M is earthquake magnitude, which in most cases is represented by the local magnitude M_L (Richter, 1958); $\log_{10} A_0(R)$ is the empirically determined function which describes attenuation versus distance (Table 1); and $a_0(M)$, $v_0(M)$, and $d_0(M)$ represent the magnitude-dependent empirical scaling functions for acceleration, velocity, and displacement.

Equation (1) is based on the assumption that $\log_{10} A_0(R)$ (Richter, 1958) describes approximately the amplitude attenuation with distance, R, for all peaks; i.e., peaks of acceleration, velocity, and displacement. It may seem at first that it is essential to have different attentuation curves for acceleration (high-frequency waves), velocity (intermediate-frequency waves), and displacement (low-frequency waves) peaks, but we found that for the limited number of data points that are available so far $\log_{10} A_0(R)$ may represent a satisfactory first-order approximation for all peaks of strong ground motion (Trifunac and Brady, 1975b) for the distance range from about 20 to 200 km.

For the scaling of peak amplitudes presented in this paper, we will neglect the dependence of $\log_{10} A_0(R)$ on wave frequency, recording site conditions, peak amplitudes, earthquake magnitude, and/or on source dimensions and will use the values of $\log_{10} A_0(R)$ which are employed in routine calculations of local magnitudes (Richter, 1958). For large earthquakes which are characterized by long faults and large peak amplitudes, the $\log_{10} A_0(R)$ curve would have a tendency to flatten out for small epicentral distances; while for low magnitude shocks which are typically not accompanied by large source dimensions and large peak amplitudes, this curve would probably have a larger negative slope for small epicentral distances than the curve we propose to use (Table 1). Such general trends would result from the properties of geometric attenuation with distance and possibly nonlinear response of soil deposits for large near-field motions. The detailed quantitative description of these effects, however, is beyond the scope of this paper, since the strong-motion data for epicentral distance less than about 20 km, which would be necessary to test the adopted attenuation laws, is completely lacking at this time.

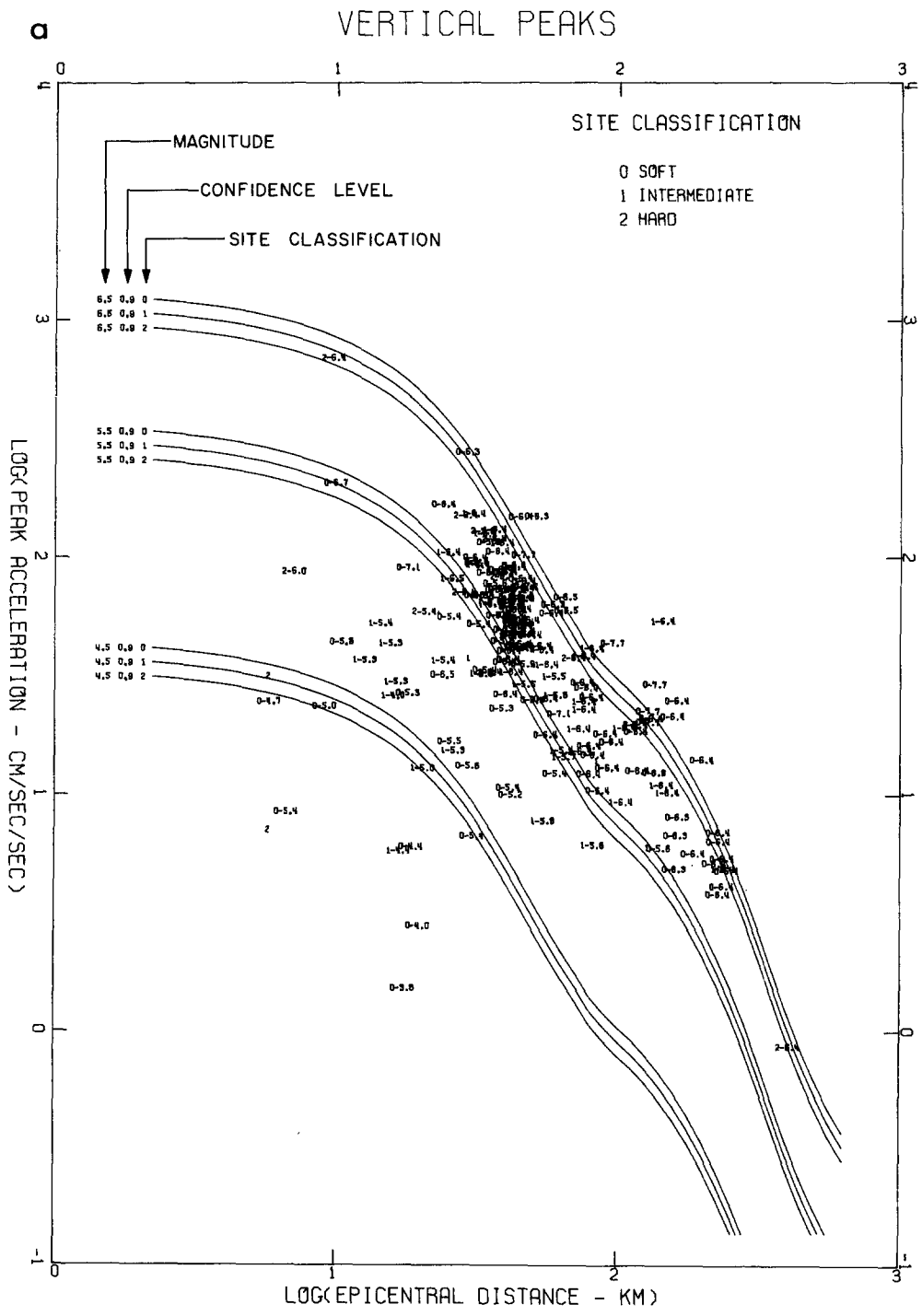

FIG. 1. Vertical and horizontal peak accelerations versus epicentral distance. Each plotted point has the site classification and magnitude, when available. Continuous lines represent the estimates of an upper bound on peak amplitudes and depend on earthquake magnitude, confidence level, and site classification.

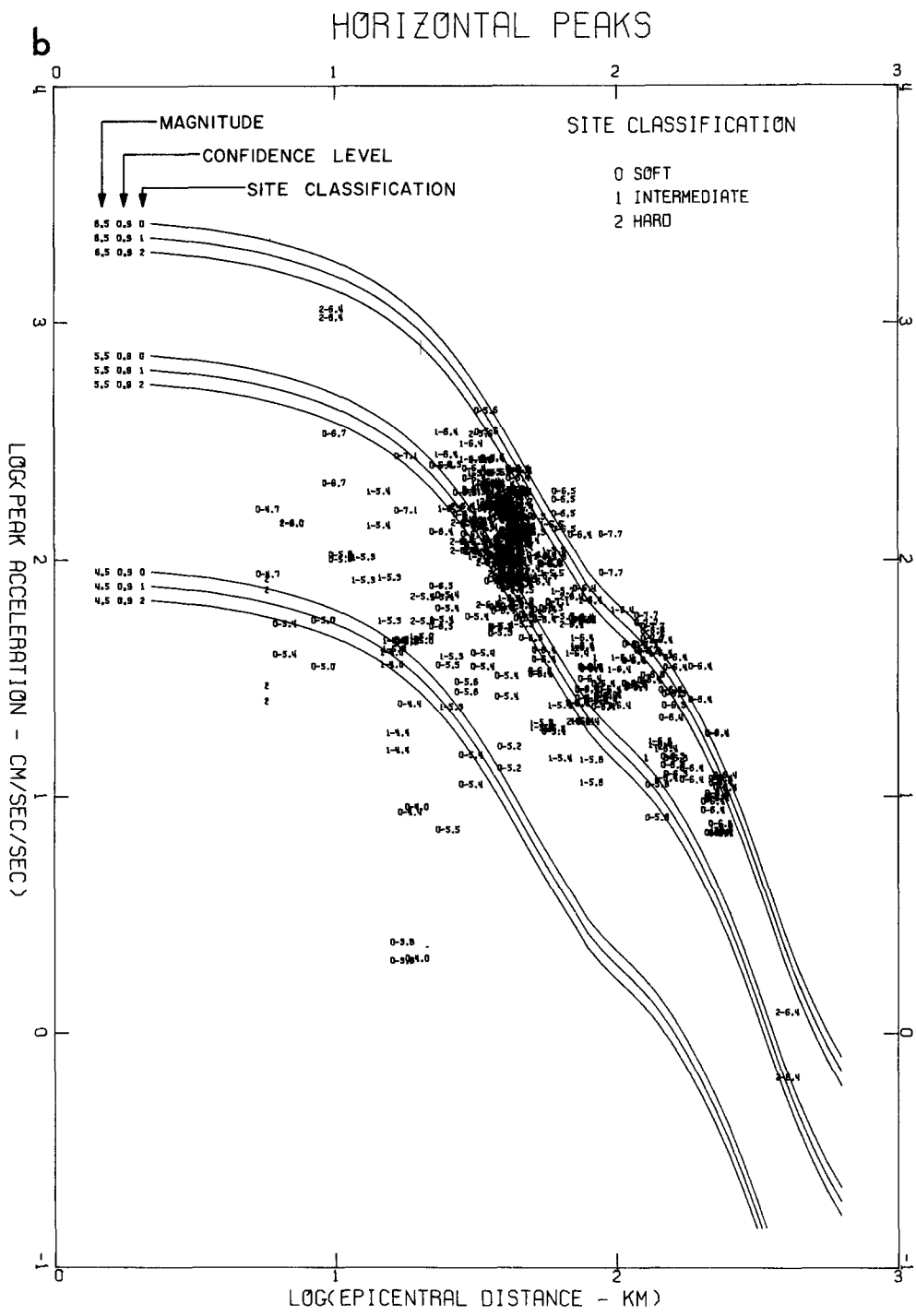

The apparent frequency-dependent attenuation of wave amplitudes associated with frequency ω and often modeled approximately by $\exp[-(\omega R/2Q\beta)]$, where R may be taken to be epicentral distance, Q is the attenuation constant, and β is the shear-wave velocity, will also be neglected in this paper. This effect may be introduced into the analysis

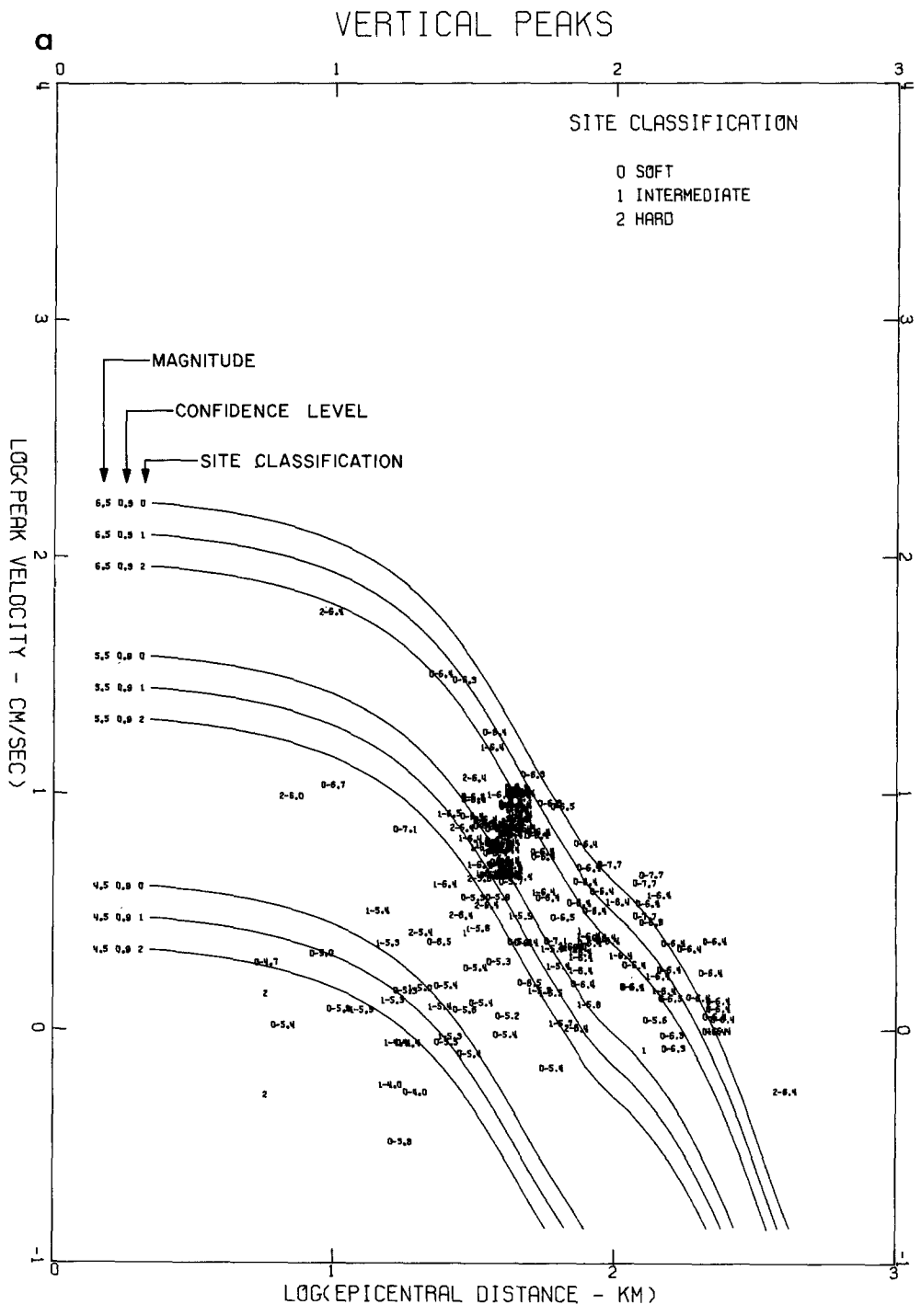

FIG. 2. Vertical and horizontal peak velocities versus epicentral distance. Each plotted point has the site classification and magnitude, when available. Continuous lines represent the estimates of an upper bound on peak amplitudes and depend on earthquake magnitude, confidence level, and site classification.

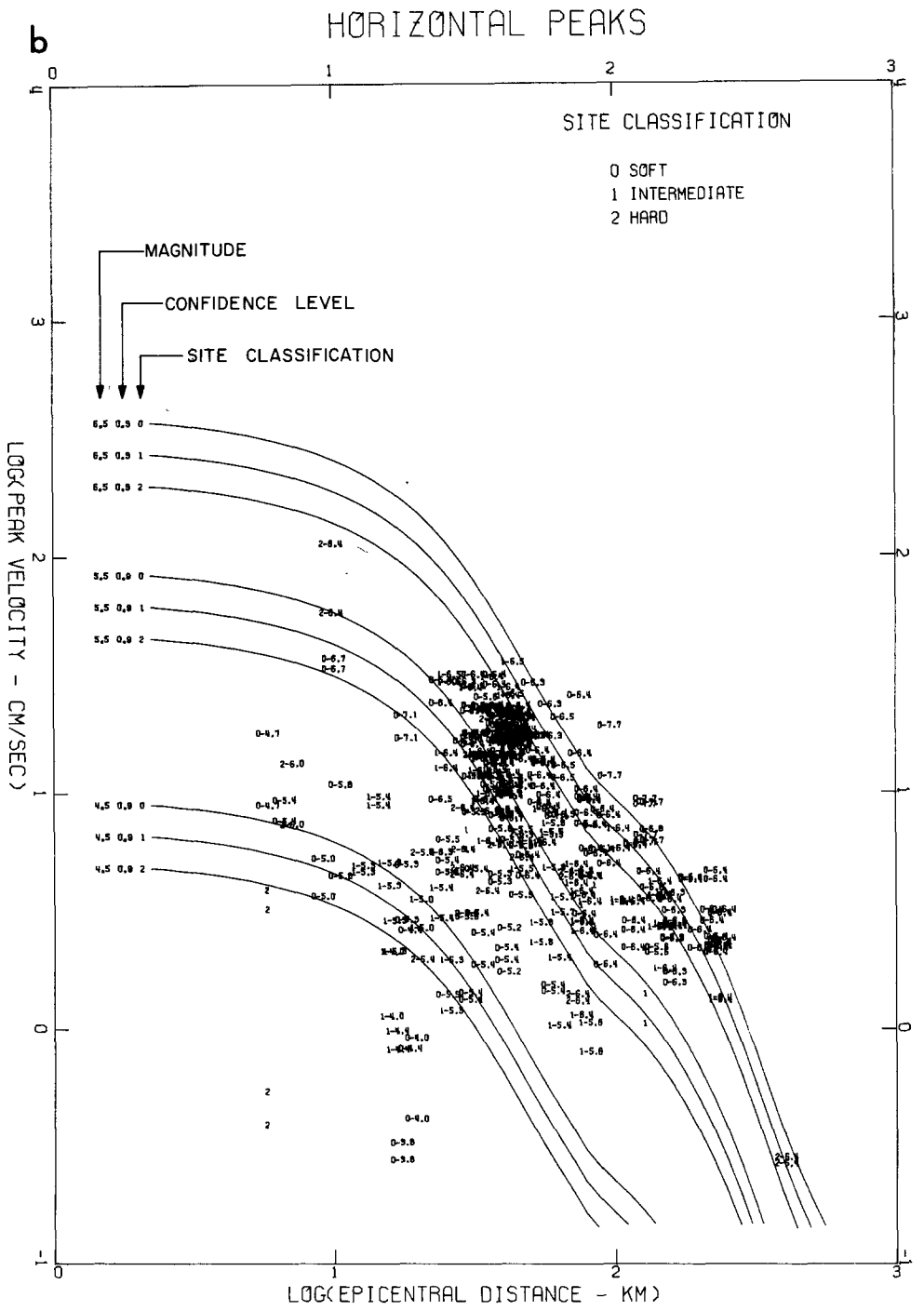

of spectral amplitudes but is difficult to incorporate into peak amplitude characterizations, since the representative frequency contents of peak amplitudes change with distance and because the relative contribution of digitization noise (Trifunac and Lee, 1974) varies with frequency and distance.

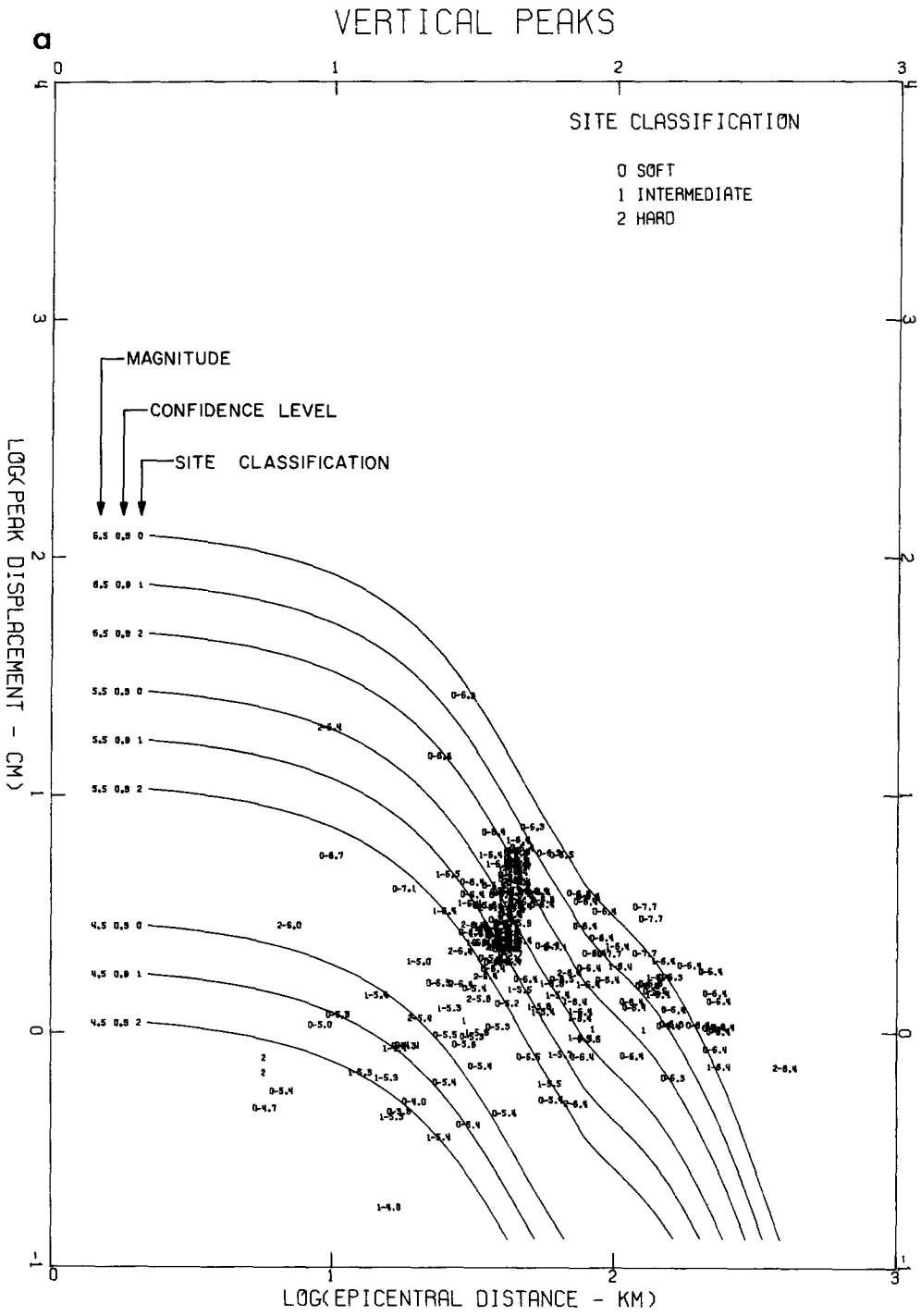

FIG. 3. Vertical and horizontal peak displacements versus epicentral distance. Each plotted point has the site classification and magnitude, when available. Continuous lines represent the estimates of an upper bound on peak amplitudes and depend on earthquake magnitude, confidence level, and site classification.

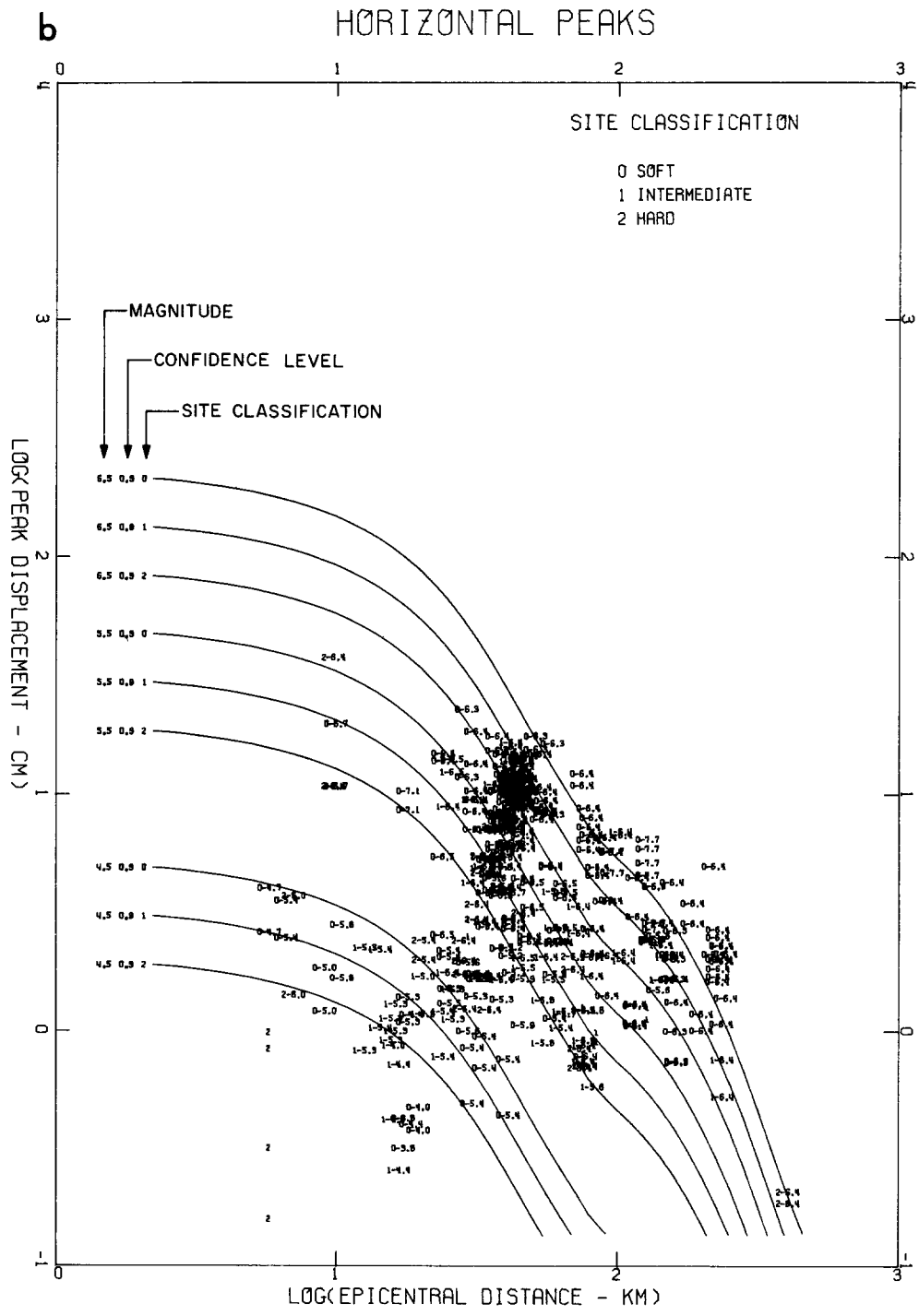

In this study the numerical values of $\log_{10} A_0(R)$ are taken to be those given by Richter (1958), and the appropriate scaling factors are included in $a_0(M)$, $v_0(M)$, and $d_0(M)$. The physical significance of $\log_{10} A_0(R)$ for our present work lies in its relative

changes of amplitude with distance which can be characterized by defining a new function $f(R)$ which is given by

$$f(R) = \log_{10} A_0(R = 0) - \log_{10} A_0(R). \tag{2}$$

TABLE 1

$\log_{10} A_0(R)$ VERSUS EPICENTRAL DISTANCE R*

R (km)	$-\log_{10} A_0(R)$	R (km)	$-\log_{10} A_0(R)$	R (km)	$-\log_{10} A_0(R)$
0	1.400	140	3.230	370	4.336
5	1.500	150	3.279	380	4.376
10	1.605	160	3.328	390	4.414
15	1.716	170	3.378	400	4.451
20	1.833	180	3.429	410	4.485
25	1.955	190	3.480	420	4.518
30	2.078	200	3.530	430	4.549
35	2.199	210	3.581	440	4.579
40	2.314	220	3.631	450	4.607
45	2.421	230	3.680	460	4.634
50	2.517	240	3.729	470	4.660
55	2.603	250	3.779	480	4.685
60	2.679	260	3.827	490	4.709
65	2.746	270	3.877	500	4.732
70	2.805	280	3.926	510	4.755
80	2.920	290	3.975	520	4.776
85	2.958	300	4.024	530	4.797
90	2.989	310	4.072	540	4.817
95	3.020	320	4.119	550	4.835
100	3.044	330	4.164	560	4.853
110	3.089	340	4.209	570	4.869
120	3.135	350	4.253	580	4.885
130	3.182	360	4.295	590	4.900

* Only the first two digits may be assumed to be significant.

Figure 4 shows a plot of $f(R)$ versus epicentral distance, R, and how it can be approximated by two straight line segments which are given by

$$f(R) = \begin{cases} R/50 & \text{for } R \leqq 75 \text{ km} \\ 1.125 + R/200 & \text{for } 350 \geqq R \geqq 75 \text{ km} \end{cases} \tag{3}$$

The change of slope at $R = 75$ km reflects the fact that for greater distances the main contribution to strong shaking comes from surface waves, which are attenuated less rapidly ($\sim 1/R^{\frac{1}{2}}$) than the near-field and intermediate-field ($\sim 1/R^{2-4}$), or far-field body waves ($\sim 1/R$). The function $f(R)$ in Figure 4 has been derived from Table 1 which represents a smoothed version of a similar table presented by Richter (1958). The third and fourth decimal places in this table have no significance and are kept only to preserve the smoothness of $A_0(R)$ amplitudes when plotted versus R. The reliability of shape and amplitudes of $\log_{10} A_0(R)$, i.e. $f(R)$, curves for epicentral distances less than about 10 km is not known, since at these short distances standard Wood-Anderson instruments go off scale for moderate and large earthquakes and the adequate number of strong-motion recordings is completely lacking there as well.

It is important to note here that $\log_{10} A_0(R)$ is of special value for the scaling functions studied in this paper because it incorporates empirically the average amplitude attenuation with distance in the Southern California Region and thus experimentally includes

the average properties of the Earth's crust in this area. Since most strong-motion data have been recorded in the same area, this curve represents the most natural first approximation to be used for scaling the strong-motion data as well. While it appears that this amplitude attenuation law might also be applied in other parts of the Western United States, it cannot be used for Central and Eastern United States (Nuttli, 1973).

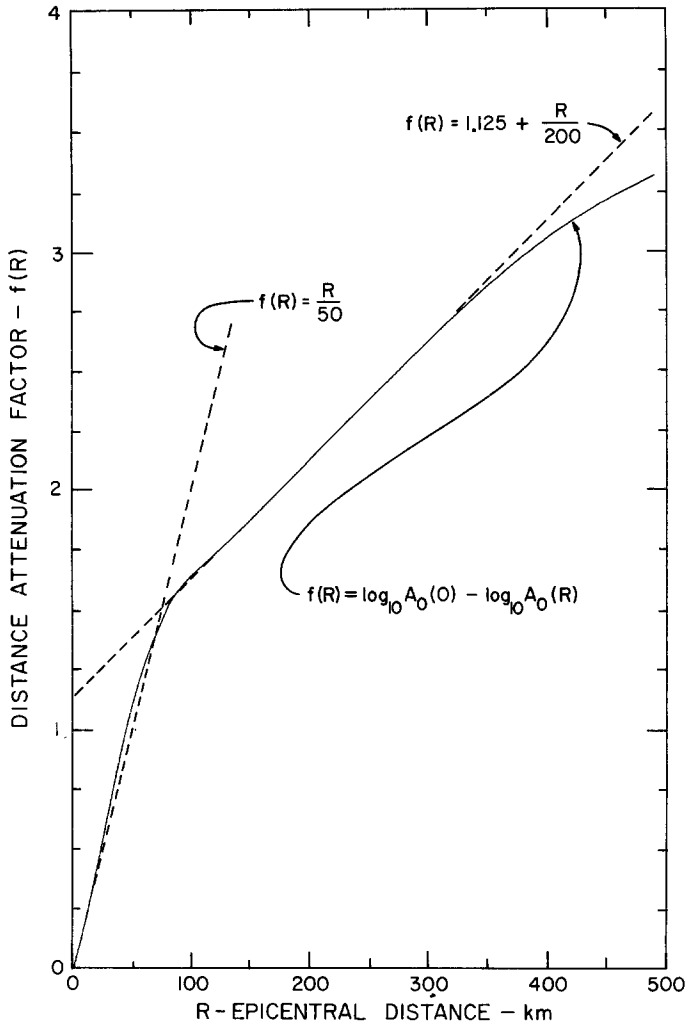

FIG. 4. Distance attenuation factor $f(R)$.

To extend the applicability of equation (1) so that it can be used for approximate scaling of the peaks of strong ground motion when the confidence with which such an estimate is made has been specified one can write

$$\log_{10}\begin{Bmatrix} a_{\max,p} \\ v_{\max,p} \\ d_{\max,p} \end{Bmatrix} = M + \log_{10} A_0(R) - \log_{10}\begin{Bmatrix} a_0(M,p,s,v) \\ v_0(M,p,s,v) \\ d_0(M,p,s,v) \end{Bmatrix}, \tag{4}$$

where M is earthquake magnitude; p is the confidence level associated with the approximate bounds $a_{\max,p}$, $v_{\max,p}$, and $d_{\max,p}$ for the peaks $a_{\max}$, $v_{\max}$, and $d_{\max}$; s represents the type of site conditions ($s = 0$ for alluvium deposits; $s = 1$ for "intermediate" rock;

TABLE 2

A COMPRESSED VERSION OF DATA TABULATED FOR THE FOUR MAGNITUDE INTERVALS

$$\text{AMPLITUDES OF } \log_{10}\begin{Bmatrix} a_0(M,p,s,v) \\ v_0(M,p,s,v) \\ d_0(M,p,s,v) \end{Bmatrix} = M+\log_{10}A_0(R)-\log_{10}\begin{Bmatrix} a_{\max,\,p} \\ v_{\max,\,p} \\ d_{\max,\,p} \end{Bmatrix}$$

Confidence Level p	Magnitude Range 4.0–4.9				Magnitude Range 5.0–5.9						Magnitude Range 6.0–6.9						Magnitude Range 7.0–7.9	
	Site class. $s=0$		Site class. $s=1$		Site class. $s=0$		Site class $s=1$		Site class. $s=2$		Site class. $s=0$		Site class. $s=1$		Site class. $s=2$		Site class. $s=0$	
	vert. $v=1$	hor. $v=0$	vert. $v=1$	hor. $v=0$	vert. $v=1$	hor. $v=0$	vert. $v=1$	hor. $v=0$	vert. $v=1$	hor. $v=0$	vert. $v=1$	hor. $v=0$	vert. $v=1$	hor. $v=0$	vert. $v=1$	hor. $v=0$	vert. $v=1$	hor. $v=0$
					Acceleration $a_0(M,p,s,v)$													
0.10					2.55	2.20	2.38	1.98			2.54	2.22	2.56	2.18	2.73	2.37		3.14
0.15																	3.38	
0.20		1.89			2.46	2.10	2.20	1.92			2.39	2.14	2.45	2.10	2.55	2.31		3.13
0.25				1.48						1.84								
0.30					2.10	1.79	2.10	1.76			2.34	2.08	2.43	2.04	2.52	2.30	3.31	2.95
0.35	1.84	1.69																
0.40					1.97	1.70	2.08	1.69			2.30	2.02	2.36	1.99	2.43	2.24		2.93
0.45																	3.26	
0.50		1.25	1.91	1.40	1.76	1.65	1.99	1.61	1.81	1.74	2.24	1.95	2.29	1.97	2.34	2.22		2.87
0.55																		
0.60					1.72	1.51	1.98	1.57			2.18	1.90	2.22	1.94	2.25	2.17	3.22	2.84
0.65																		
0.70	1.80	1.25			1.69	1.38	1.94	1.43			2.13	1.84	2.18	1.91	2.22	1.98		2.82
0.75				0.73						1.07							3.11	
0.80					1.53	1.16	1.86	1.34			2.04	1.71	2.11	1.85	2.14	1.88		2.80
0.85		1.24																
0.90					1.40	0.85	1.65	1.17			1.87	1.59	2.08	1.76	2.10	1.79	3.11	2.64

Velocity $v_0(M, p, s, v)$

0.10					3.85	3.20	3.57	3.25			3.44	3.13	3.60	3.26	3.92	3.72	4.50	4.12
0.15																		
0.20		2.71			3.50	3.01	3.46	3.04			3.37	3.02	3.51	3.12	3.72	3.64		4.11
0.25				2.76						3.29								
0.30					3.29	2.86	3.39	2.96			3.33	2.90	3.32	3.00	3.61	3.47	4.49	4.01
0.35	2.90	2.59																
0.40					3.15	2.81	3.28	2.89			3.14	2.84	3.27	2.92	3.54	3.40	4.09	3.78
0.45																		
0.50		2.24	2.73	2.68	3.10	2.70	3.21	2.76	3.17	2.84	3.09	2.79	3.26	2.85	3.41	3.29		3.74
0.55																		
0.60					2.95	2.52	3.11	2.73			3.04	2.72	3.18	2.82	3.37	3.17	4.08	3.68
0.65																		
0.70	2.68	2.24			2.78	2.42	2.99	2.63			2.95	2.68	3.16	2.77	3.35	3.08	4.05	3.62
0.75				2.23						2.33								
0.80					2.67	2.32	2.83	2.50			2.81	2.53	3.03	2.73	3.27	2.91		3.58
0.85		2.21																
0.90					2.37	2.06	2.66	2.44			2.72	2.36	2.97	2.64	3.04	2.60	3.95	3.55

Displacement $d_0(M, p, s, v)$

0.10					4.12	3.58	3.95	3.70			3.80	3.44	3.90	3.65	4.19	4.30	4.73	4.50
0.15																		
0.20		3.02			3.69	3.46	3.94	3.58			3.72	3.30	3.81	3.53	4.06	4.16		4.41
0.25				3.26						3.28								
0.30					3.59	3.34	3.78	3.48			3.65	3.21	3.67	3.42	4.01	4.02	4.62	4.33
0.35	3.51	2.77																
0.40					3.42	3.29	3.71	3.37			3.43	3.08	3.59	3.25	4.01	3.89	4.42	4.11
0.45																		
0.50		2.62	3.03	2.81	3.25	3.11	3.26	3.18	3.52	3.20	3.31	3.01	3.51	3.18	3.88	3.78		4.08
0.55																		
0.60					3.11	3.00	3.16	3.12			3.24	2.94	3.47	3.07	3.81	3.69	4.23	4.07
0.65																		
0.70	2.68	2.58			3.06	2.75	3.11	2.95			3.10	2.87	3.40	3.04	3.70	3.49	4.09	4.03
0.75				2.66						2.83								
0.80					2.93	2.61	2.97	2.81			2.97	2.68	3.22	2.98	3.62	3.24		3.91
0.85		2.56																
0.90					2.78	2.24	2.89	2.72			2.80	2.51	3.05	2.86	3.52	2.76	4.06	3.86
No. of Data	3	6	2	4	24	47	15	30	2	4	82	164	34	68	12	24	7	14

$s = 2$ for basement rock); and v is used to describe the component direction ($v = 0$ for horizontal and $v = 1$ for vertical direction). As an approximation, we assume that the scaling functions $a_0(M, p, s, v)$, $v_0(M, p, s, v)$, and $d_0(M, p, s, v)$ can be described by

$$\log_{10} \begin{Bmatrix} a_0(M, p, s, v) \\ v_0(M, p, s, v) \\ d_0(M, p, s, v) \end{Bmatrix} = ap + bM + c + ds + ev + fM^2 \tag{5}$$

where a, b, c, d, e, and f are the coefficients which have to be determined. In this paper we shall neglect the second and higher order terms of p and s and the third and higher order terms of M, as well as the terms which include different products of p, s and M. The data we have at our disposal now are not uniformly representative for different values of the parameters s and M (e.g., 63 per cent of all data have been classified as $s = 0$ and only 8 per cent as $s = 2$, while 71 per cent of all data belong to the magnitude range from 6.0 to 6.9) so that the estimates of the coefficients of the higher order terms than those in equation (5) might be affected by this nonuniformity of the data rather than being representative of the real trends of the scaling functions a_0, v_0 and d_0.

Regression Analysis

To compute the coefficients a, b, c, d, e, and f in equation (5), it is necessary to determine the estimates of $\log_{10} [a_0(M, p, s, v)]$, $\log_{10} [v_0(M, p, s, v)]$, and $\log_{10} [d_0(M, p, s, v)]$ for different values of their arguments by using the available strong-motion data. Since there are only 181 strong-motion accelerograms that can be subdivided into the needed subgroups, it is clear that the presently available data are far from adequate to characterize the $\log_{10} [a_0(M, p, s, v)]$, $\log_{10} [v_0(M, p, s, v)]$, and $\log_{10} [d_0(M, p, s, v)]$ over a sufficiently broad range of their arguments (note that 181 rather than 187 accelerograms have been used because of incomplete availability of magnitude determinations). Nevertheless, an attempt can be made to determine a first approximation to the coefficients a, b, c, d, e and f. To do this we begin by partitioning all data into four groups that correspond to the magnitude ranges 4.0–4.9, 5.0–5.9, 6.0–6.9, and 7.0–7.9. Each of these groups is next subdivided into three subgroups which correspond to the site classifications, s ($s = 0$, 1 or 2). Depending on whether the recording component is horizontal or vertical, each of these subgroups is finally divided into two parts corresponding to $v = 0$ and $v = 1$. Within each of these parts, we calculate

$$\log_{10} \begin{Bmatrix} a_0(M, p, s, v) \\ v_0(M, p, s, v) \\ d_0(M, p, s, v) \end{Bmatrix} = M + \log_{10} A_0(R) - \log_{10} \begin{Bmatrix} a_{\max} \\ v_{\max} \\ d_{\max} \end{Bmatrix}. \tag{6}$$

An array of n data points in one such part can be further arranged so that the numerical values of $\log_{10} [a_0(M, p, s, v)]$, $\log_{10} [v_0(M, p, s, v)]$, and $\log_{10} [d_0(M, p, s, v)]$ decrease monotonically with increasing n. Then, if m = integer part of (pn), the mth data point will represent an estimate for an upper bound of $\log_{10} [a_0(M, p, s, v)]$, $\log_{10} [v_0(M, p, s, v)]$, or $\log_{10} [d_0(M, p, s, v)]$, which is associated with the p-per cent confidence level. Table 2 presents a compressed version of such data tabulated for the four magnitude intervals, and indicates the number of data points used in their estimates. For actual calculations we used the confidence levels equal to 0.5, 0.10, 0.15, . . ., 0.85, 0.90, and 0.95 and the reported magnitudes corresponding to each individual estimate of $\log_{10} [a_0(M, p, s, v)]$, $\log_{10} [v_0(M, p, s, v)]$, and $\log_{10} [d_0(M, p, s, v)]$ whenever the number of data points within each part permitted such detailed classification.

Table 3 presents the results of least-squares fitting of equations (5) to the above data. It presents the estimates of the coefficients $a, b, \ldots, e$, and f; the total number of data points which have been used in the fitting; and the $M_{\min}$ and $M_{\max}$, which are the lowest and the highest magnitudes for which equations (5) are assumed to apply.

The curves $\log_{10}[a_0(M, p, s, v)]$, $\log_{10}[v_0(M, p, s, v)]$, and $\log_{10}[d_0(M, p, s, v)]$ represent parabolas when plotted versus M. Their amplitudes depend on p, s, and v. As far as their functional form is concerned, it should be noted here, however, that there is no direct physical justification for such parabolic dependence, and that this choice is motivated by the simplicity of its mathematical form and the apparent trend of data indicated by our previous analyses (Trifunac and Brady, 1975b). Since this overall trend of data suggests that the amplitudes of $\log_{10}[a_0(M, p, s, v)]$, $\log_{10}[v_0(M, p, s, v)]$, and $\log_{10}[d_0(M, p, s, v)]$ might level off for some small magnitude, we have decided, quite

TABLE 3

COEFFICIENTS IN THE EXPRESSION*

$$\log_{10}\begin{Bmatrix} a_0(M,p,s,v) \\ v_0(M,p,s,v) \\ d_0(M,p,s,v) \end{Bmatrix} = \begin{cases} ap+bM+c+ds+ev+fM^2-f(M-M_{\max})^2 & \text{for } M \geqq M_{\max} \\ ap+bM+c+ds+ev+fM^2 & \text{for } M_{\max} \geqq M \geqq M_{\min} \\ ap+bM_{\min}+c+ds+ev+fM^2{}_{\min} & \text{for } M \leqq M_{\min} \end{cases}$$

Function	a	b	c	d	e	f	N Data	$M_{\min}$	$M_{\max}$
$\log_{10}a_0(M, p, s, v)$	−0.898	−1.789	6.217	0.060	0.331	0.186	227	4.80	7.50
$\log_{10}v_0(M, p, s, v)$	−1.087	−2.059	8.357	0.134	0.344	0.201	227	5.12	7.61
$\log_{10}d_0(M, p, s, v)$	−1.288	−2.366	9.717	0.205	0.240	0.226	227	5.24	7.45

* Only the first two digits may be assumed to be significant.

arbitrarily, to adopt equations (5) for $M \geqq M_{\min}$, where $M_{\min}$ is that value of M for which the minima of the above functions are achieved and to use the constant amplitudes equal to these minima for $M \leqq M_{\min}$. $M_{\max}$ is defined as the point where the parabola reaches unit slope, equal to the slope of M in equation (4), and for $M \geqq M_{\max}$ the right-hand side of (5) continues linearly with this slope. This can be summarized as follows

$$\log_{10}\begin{Bmatrix} a_0(M,p,s,v) \\ v_0(M,p,s,v) \\ d_0(M,p,s,v) \end{Bmatrix} = \begin{cases} ap+bM+c+ds+ev+fM^2-f(M-M_{\max})^2 & \text{for } M \geqq M_{\max} \\ ap+bM+c+ds+ev+fM^2 & \text{for } M_{\max} \geqq M \geqq M_{\min} \\ ap+bM_{\min}+c+ds+ev+fM^2_{\min} & \text{for } M \leqq M_{\min} \end{cases} \quad (7)$$

and means that the maxima of $a_{\max}$, $v_{\max}$ and $d_{\max}$ are attained for $M \geqq M_{\max}$.

The values of the coefficients in equation (7) are shown in Table 3 where only the two first digits may be taken as significant. The confidence level coefficient "a" tends to increase slightly from acceleration to velocity and displacement indicating somewhat greater scatter of peak displacements, poorer fit of displacements to the $\log_{10}A_0(R)$ curve, a slight overestimate of maximum displacement peaks for large epicentral distances caused by digitization processing noise (computed displacement peaks which are equal to or less than several centimeters in most cases are contaminated by noise, Trifunac and Lee, 1974), or, most probably, some combination of all these effects. The values of site

coefficient "d" approximately double from acceleration to velocity and from velocity to displacement, reflecting progressively greater importance of site conditions on peak amplitudes of longer period waves. The same effect is also illustrated in Figures 1, 2, and 3 where the continuous confidence levels for $M = 4.5$, 5.5, and 6.5 for $p = 0.9$ and for $s = 0$, 1 and 2 which are calculated from the coefficients in Table 3 have been presented. These results thus indicate that for a given confidence level the peak acceleration is influenced only to a small degree by the site conditions and that it is about 30 per cent larger for alluvium site conditions ($s = 0$) than for rock sites ($s = 2$). The corresponding difference for peak displacements, however, is equal to 250 per cent.

In our previous work dealing with the correlations of peak accelerations with Modified Mercalli Intensity (Trifunac and Brady, 1975a) or with the correlations of peak accelera-

TABLE 4

CHECKING OF THE SUCCESS IN PEAK BRACKETING

Confidence Level	Found Peaks Less than the Limit		Found Peaks Greater than the Limit	
	No.	Fraction	No.	Fraction
$p = 0.9$	1566	0.930	117	0.070
$p = 0.8$	1485	0.881	198	0.119
$p = 0.7$	1345	0.800	338	0.200
$p = 0.6$	1172	0.696	511	0.314
$p = 0.5$	976	0.578	707	0.422
$p = 0.4$	743	0.440	940	0.560
$p = 0.3$	505	0.300	1178	0.700
$p = 0.2$	327	0.194	1356	0.806
$p = 0.1$	215	0.127	1468	0.873

Total no. of peaks = 1683*

* Acceleration, velocity and displacement peaks were lumped together. One vertical and two horizontal peaks were also lumped together.

tions with earthquake magnitude and epicentral distance for moderate and small magnitudes (Trifunac and Brady, 1975b), we found that the different site conditions had no significant effect on the recorded peaks but that there exists a tendency for a slight, yet consistent, increase of peak amplitudes for harder sites ($s = 2$). These investigations deal with the amplitudes of the expected peaks, while the present paper investigates the approximate bounds of peak amplitudes. In view of the fact that we do expect to find the largest standard deviations for the peak amplitudes recorded on alluvium sites and because we employ $\log_{10} A_0(R)$ which does not depend on site conditions, it is not surprising that in this approximate analysis we find the overall bounds for peak accelerations to be slightly higher on alluvium than on hard-rock sites. Simple, two-dimensional theoretical studies, which are based on linear models, for example, show that the average peak accelerations on alluvium do not change much but that the variations from the mean grow rapidly with a decrease of wavelength and an increase in velocity contrast across a material discontinuity (e.g., Trifunac, 1971; Wong and Trifunac, 1974). Nevertheless, when more records become available at small distances from faults, we will most probably find that in the near-field the high-frequency large peak amplitudes will tend to be smaller on alluvium ($s = 0$) than on hard-rock sites ($s = 2$) because the peak amplitudes

that can be transmitted through the alluvium and soil deposits will be limited by the nonlinear response of these materials.

The value of coefficient "e" in Table 3 is close to 0.3 and shows that $a_{\max,p}$, $v_{\max,p}$ and $d_{\max,p}$ for horizontal peaks are about twice as large as the corresponding levels for vertical peaks. This is in fair agreement with the trends indicated by the average peak amplitudes (Trifunac and Brady, 1975b) in similar correlations with earthquake magnitude and epicentral distance and in related correlations with the Modified Mercalli Intensity Scale (Trifunac and Brady, 1975a).

The above description of $a_0(M, p, s, v)$, $v_0(M, p, s, v)$ and $d_0(M, p, s, v)$ involves several oversimplifying assumptions and should therefore be evaluated critically. To do this we calculated $a_{\max,p}$, $v_{\max,p}$, and $d_{\max,p}$ for the parameters that correspond to those

TABLE 5

HORIZONTAL PEAK DISPLACEMENTS—$\log_{10}[d_{\max}(R = 0)]$ ($d_{\max}$ IS IN CENTIMETERS)*

Site Classification	$p = 0.5$	$p = 0.6$	$p = 0.7$	$p = 0.8$	$p = 0.9$
		$M = 7.5$			
0	2.06	2.19	2.32	2.45	2.58
1	1.86	1.98	2.11	2.24	2.37
2	1.65	1.78	1.91	2.04	2.17
		$M = 6.5$			
0	1.86	1.99	2.12	2.44	2.37
1	1.65	1.78	1.91	2.04	2.17
2	1.45	1.58	1.71	1.83	1.96
		$M = 5.5$			
0	1.20	1.33	1.46	1.59	1.72
1	1.00	1.13	1.26	1.38	1.51
2	0.79	0.92	1.05	1.18	1.31
		$M = 4.5$			
0	0.22	0.35	0.48	0.61	0.73
1	0.014	0.14	0.27	0.40	0.53
2	−0.19	−0.062	0.067	0.20	0.32

* Only the first two digits may be assumed to be significant.

for all components of recorded peak acceleration, velocity, and displacement and for nine confidence levels equal to 0.1, 0.2, . . ., 0.8, and 0.9. For every confidence level this amounts to comparing 1683 data points with the calculated bounds $a_{\max,p}$, $v_{\max,p}$, and $d_{\max,p}$ and tabulation of the percentage of recorded peaks that are actually below or above the computed bounds. It one pools all peaks together, then this comparison is as indicated in Table 4. This table shows that in all but one case for $p = 0.2$ the number of peaks below the corresponding bound is equal to or greater than that required by the percentage equal to p. Consequently, it may be concluded from this test that the above simplifying assumptions are acceptable for derivation of approximate bounds of the currently available peaks of strong ground motion.

Tables 5, 6, and 7 and Figure 4 enable one to calculate quickly the logarithms for the approximate bounds on peak acceleration, velocity, and displacement by subtracting the

TABLE 6

HORIZONTAL PEAK VELOCITIES—$\log_{10}[v_{max}(R = 0)]$ (v_{max} IS IN CENTIMETERS PER SECOND)*

Site Classification	$p = 0.5$	$p = 0.6$	$p = 0.7$	$p = 0.8$	$p = 0.9$
		$M = 7.5$			
0	2.42	2.53	2.64	2.75	2.85
1	2.95	2.39	2.47	2.61	2.72
2	2.15	2.26	2.37	2.48	2.58
		$M = 6.5$			
0	2.18	2.29	2.40	2.50	2.61
1	2.04	2.15	2.26	2.37	2.48
2	1.91	2.02	2.13	2.24	2.34
		$M = 5.5$			
0	1.53	1.63	1.75	1.86	1.97
1	1.40	1.50	1.61	1.72	1.83
2	1.26	1.37	1.48	1.56	1.70
		$M = 4.5$			
0	0.560	0.668	0.777	0.885	0.994
1	0.425	0.534	0.643	0.751	0.860
2	0.291	0.400	0.509	0.618	0.726

* Only the first two digits may be assumed to be significant.

TABLE 7

HORIZONTAL PEAK ACCELERATIONS—$\log_{10}[a_{max}(R = 0)]$ (a_{max} IS IN CENTIMETERS PER SECOND PER SECOND)*

Site Classification	$p = 0.5$	$p = 0.6$	$p = 0.7$	$p = 0.8$	$p = 0.9$
		$M = 7.5$			
0	3.29	3.38	3.47	3.56	3.65
1	3.23	3.32	3.41	3.50	3.59
2	3.17	3.26	3.35	3.44	3.53
		$M = 6.5$			
0	3.10	3.19	3.28	3.37	3.46
1	3.04	3.13	3.22	3.31	3.40
2	2.98	3.07	3.16	3.25	3.34
		$M = 5.5$			
0	2.54	2.63	2.72	2.81	2.90
1	2.49	2.57	2.66	2.75	2.84
2	2.42	2.51	2.60	2.69	2.78
		$M = 4.5$			
0	1.63	1.72	1.81	1.90	1.99
1	1.57	1.66	1.75	1.84	1.93
2	1.51	1.60	1.69	1.78	1.87

* Only the first two digits may be assumed to be significant.

value for $f(R)$ at a selected distance from an appropriate entry in Tables 5, 6, or 7. Formally, Tables 5, 6, and 7 represent the estimates of bounds on maximum peak acceleration, velocity, and displacement at $R = 0$. However, as we already pointed out, since the adequacy of $\log_{10} A_0(R)$ for R less than 10 to 20 km cannot be tested critically because there is virtually no strong-motion data for these short distances, the entries in Tables 5, 6, and 7 can, so far, only be interpreted to represent the scaling factors for use with $f(R)$ and are valid for approximate scaling of peaks only for R between about 20 and 200 km.

Comparison of the Empirically Determined Peak Amplitudes with those Derived from Source Mechanism Studies

In the above analysis we have presented scaling relationships for peaks of acceleration, velocity, and displacement for the assumed empirical law of attenuation versus distance given by $\log_{10} A_0(R)$ (Richter, 1958). As shown in the previous study (Trifunac and Brady, 1975b), this attenuation law represents an acceptable approximation to the observed amplitude variations with distance for epicentral distances ranging from about 20 km to about 200 km. Although Richter (1958) presents the curve $\log_{10} A_0(R)$ for distances ranging from 0 km to well over 600 km, at the present time there is not enough recorded strong-motion data for distances less than 20 km or greater than 200 km to test whether this same attenuation law can be extended outside the range for which we have already suggested its approximate validity. Our next aim is, therefore, to examine whether the extrapolation is permissible and under what conditions, if any, the above-developed scaling laws may be used for the interim prediction of peaks at distances which are less than 20 km before more accurate attenuation laws become available. Testing of such an extension is clearly more important for distance less than 20 km than it is at distances greater than 200 km because there is a lack of recorded data at small distances where the peak accelerations will be largest.

In the following three sections we make an attempt to examine the plausibility of extrapolating the above-developed scaling laws back to zero epicentral distance. We do this by comparing the peaks predicted by our present analysis with other independent calculations derived from several source mechanism studies which were carried out in the same geographic area in which the strong-motion accelerograms have been recorded.

In all calculations in this paper we use epicentral rather than hypocentral or closest distance to the fault. While this is a necessary simplification, since the fault depths and orientations are accurately known for only a few earthquakes studied in this paper, the flattening nature of $\log_{10} A_0(R)$ for R small and the fact that most earthquakes in California have hypocentral depth less than 15 km seem to justify this approximation. In any case, peak amplitudes of the near-field strong ground motion seem to result from localized and energetic motions somewhere on the fault. Since there is no reason to believe that the fault section contributing most to these peak amplitudes is located at the focus or at the point which is closest to the recording station, even if we knew the hypocentral or the distance perpendicular to the fault, it would still be difficult to justify the choice of either of these two distances as being significantly better for the present application than the epicentral distance. This is, of course, correct only if the source dimension is not much larger than the epicentral distance. For large shallow earthquakes which may be characterized by long faults the distance perpendicular to the fault would seem to be most appropriate if the fault-to-station distance is much smaller than the epicentral distance. However, since no earthquake studied in this paper unequivocally falls in this category, we chose to work with the epicentral distance only.

(*a*) *Peaks of strong-motion displacement.* Table 5 summarizes the estimates of maxi-

mum peak displacements for several different magnitudes, M, confidence levels, p, and site classifications, $s = 0$, 1, and 2. The amplitudes in this table have been derived by extrapolating from the distance range to which equation (4) applies to the epicentral distance $R = 0$.

For shallow or surface faults the maximum dynamic displacement amplitude of strong ground motion, d_{max}, would be expected to approach one-half of the maximum static dislocation amplitude, u_{max}, as $R \to 0$ if we assume that no significant overshoot of dislocation takes place. For a number of simple fault geometries (see references in Table 1 of Trifunac, 1973) the maximum static dislocation amplitude, u_{max}, and the overall average static dislocation amplitude, $\bar{u}$, are approximately related by

$$\bar{u} \approx \frac{3}{4} u_{max}. \tag{8}$$

Consequently, we have

$$\bar{u} \approx \frac{3}{2} d_{max}. \tag{9}$$

The plausibility of this statement may be based on the fact that the frequencies associated with ground displacement are low and that the main contribution to the displacement amplitudes for small R comes from the near-field terms in the DeHoop's Representation Theorem (Haskell, 1969) in which the relative motion on the fault dominates the characteristics of displacements in the vicinity of the fault. On the other hand, the weakness of this statement is related to the fact that the "static" fault displacement, $\bar{u}$, is being correlated with the "observed dynamic" peak displacement from which all the periods longer than about 15 sec have been filtered out (Trifunac and Lee, 1974), Consequently, in the near-field and for large earthquakes the "observed dynamic" peak displacement, d_{max}, may be smaller than the actual peak displacement because of the limitations imposed by the currently available methods for double integration of recorded accelerograms (Trifunac and Lee, 1974).

Source mechanism studies based on spectra of recorded P and S waves (e.g., Brune, 1970; Hanks and Wyss, 1972; Trifunac, 1972a, 1972b) usually characterize an earthquake source in terms of two independent static parameters which are often selected to be: (1) Seismic moment, M_0, and (2) source dimension, r. The seismic moment is defined by

$$M_0 = \mu \bar{u} A, \tag{10}$$

where μ is the rigidity constant in the source region, $\bar{u}$ is the average dislocation amplitude, and A is the area of fault. Assuming that the fault area can be approximated by a disk of radius r, i.e. $A = \pi r^2$, from a known M_0 and r, one can calculate an estimate of the average dislocation $\bar{u}$ as follows

$$\bar{u} = \frac{M_0}{\mu \pi r^2}. \tag{11}$$

This result can be employed for comparison of the expected static displacements, $\bar{u}$, in the source region with the estimates of $\bar{u}$, using equation (9), compiled from dynamic displacement maxima which are calculated from strong-motion data at distance and by extrapolating back to $R = 0$ on the basis of equation (4) an Tables 1 and 3.

Figure 5 presents such a comparison for an average dislocation amplitude, $\bar{u}$, plotted versus local magnitude, M_L. The data representing $\bar{u}$ have been calculated from Table 1 of Thatcher and Hanks (1973) and by using equation (11). Additional data derived from the

source mechanism studies based on strong-motion accelerograms have been derived from Tables 1 and 3 of Trifunac (1972a) and Tables 1 and 2 of Trifunac (1972b). It can be seen from this figure that, although the data scatter is considerable, there is a general trend for dislocation amplitudes to increase for larger earthquake magnitudes.

Continuous curves in Figure 5 represent the amplitudes of $\bar{u}$ computed from equation (9) for $d_{\max,p}$ with the confidence levels $p = 0.5$ and 0.9 and for the two site classifications $s = 0$ and $s = 2$. By comparing the overall trend of $\bar{u}$ data with these continuous lines, we find that they are in good agreement considering the number of uncertainties in the analysis and the simple approximations employed.

For the computation of $\bar{u}$ from the data of Thatcher and Hanks (1973), we used $\mu = 3 \times 10^{11}$ dyne/cm^2 in equation (11) and made no attempt to use lower values of μ for shallow or surface sources. More detailed analyses and classifications of Thatcher and

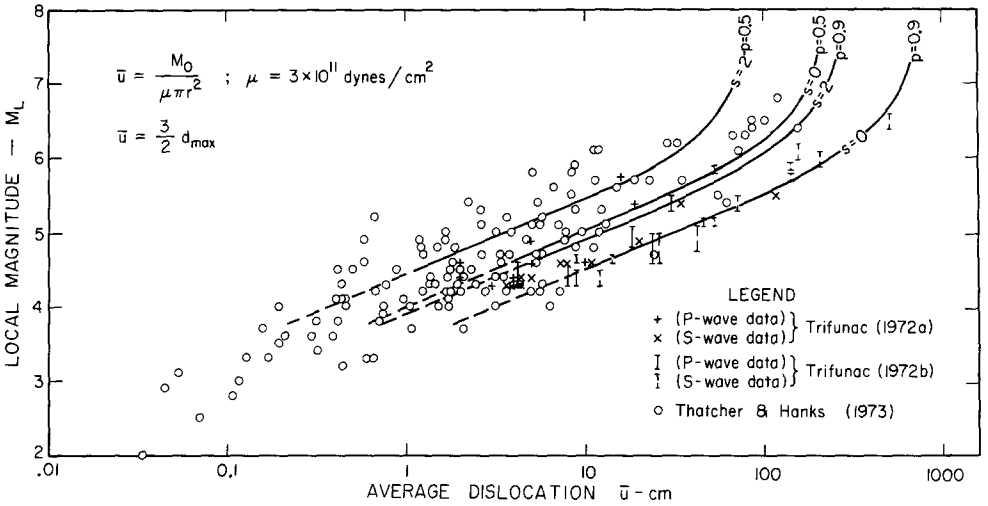

FIG. 5. Comparison of average dislocation amplitudes, $\bar{u}$, derived from three source mechanism studies (points) with amplitudes computed from statistical analysis of strong-motion data (lines).

Hanks' (1973) data, as well as our results based on strong-motion data (Trifunac, 1972a, 1972b), might reduce the overall scatter of points in Figure 5. Nevertheless, the agreement between the approximate inferences based on equations (9) and (11) and the analysis of peak amplitudes at $R = 0$ appears to be good. We interpret this agreement to mean that the empirical scaling and attenuation laws for peak displacements incorporated into equation (4) can be extended to apply for epicentral distances between 0 and 20 km.

(*b*) *Peaks of strong-motion velocity.* To test the amplitudes of peak velocities computed from equation (4) for epicentral distance $R = 0$, one may choose to work with another quantity which can be directly related to peak velocity, i.e., effective stress σ (Brune, 1970). This approach seems to represent the only alternative at this time because most observational source mechanism studies tabulate only the effective stress or stress drop as one of the basic parameters which could be related to the particle velocity at source (e.g., Brune, 1970; Hanks and Wyss, 1972; Thatcher and Hanks, 1973; Trifunac, 1972a, 1972b).

Using a one-dimensional analog of faulting in an infinite homogeneous space, Brune (1970) showed that the peak particle velocity in the near-field, v, the effective stress, σ (effective stress is the difference between initial static stress and frictional shear stress on the fault during rupture. A different kind of "stress drop" is represented by the difference

between the initial and final static stresses. For simplicity in this paper, these two different quantities will often be referred to simply as "stress drop"), the shear-wave velocity, β, and the material rigidity in the source region, μ, are all approximately related by

$$v(R = 0) \approx \sigma\beta/\mu. \tag{12}$$

If one estimates β and μ and assumes that $v \approx v_{max}$, where we are not including a correction for the reflection off the half-space since, at $R = 0$, v_{max} is the peak velocity recorded at the shallow or surface fault, then

$$\sigma \approx v_{max}(R = 0)\,\mu/\beta. \tag{13}$$

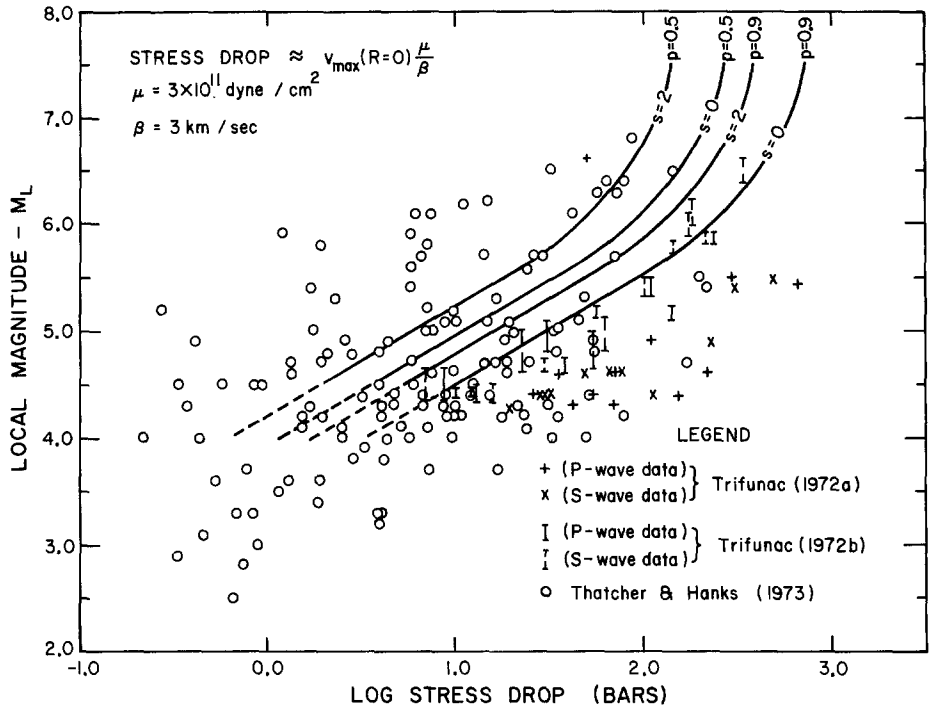

FIG. 6. Comparison of the estimates of stress drop computed in three source mechanism studies (points) with the estimates based on statistical analysis of strong-motion data (lines).

For $\beta \sim 3$ km/sec and $\mu = 10^{11}$ dynes/cm^2 to 3×10^{11} dynes/cm^2, equation (12) gives 1 to 3 cm/sec per one bar of stress drop. This range of peak amplitudes appears to be in good agreement with the work of Dietrich (1973) (Figure 5 in his paper) who parametrized peak velocity and distance by using stress drop and minimum rupture dimension in his finite element modeling of near-field ground motion.

With values of $\mu = 3 \times 10^{11}$ dynes/cm^2 and $\beta = 3$ km/sec, equations (4) and (13) can be combined to plot the corresponding estimates of confidence levels for the stress drop versus local earthquake magnitude M_L. Such plots are presented in Figure 6 for site classifications $s = 0$ and $s = 2$ and for two confidence levels $p = 0.5$ and $p = 0.9$. Here again, we are not using the lower values of μ for shallow sources, because for most data points in Figure 6 which are derived from the studies of Thatcher and Hanks (1973) and Trifunac (1972a, b) the source geology is not known in detail and because these investigators used $\mu = 3 \times 10^{11}$ dynes/cm^2 for the majority of their calculations. Since μ enters as a scaling constant in equations (11) and (13) in the same manner for both the source

mechanism studies as well as for the scaling laws studied in this paper, so long as we use the same numerical values in both calculations, the relative comparisons of the two will not be affected.

In addition to the estimates of stress drop from equations (4) and (13), Figure 6 presents the data on stress drop versus magnitude, M_L, derived from the studies by Thatcher and Hanks (1973), Trifunac (1972a), and Trifunac (1972b). All of these data have been computed by using the approximate spectral theory proposed by Brune (1970) and represent the stress drop or the effective stress that can be computed from the high-frequency amplitudes of *P*- and *S*-wave displacement spectra. For this reason such estimates represent, at best, only an overall average of what may be a rapidly varying stress over the fault plane and consequently may be subject to large fluctuations. For example, for aftershocks of a large earthquake, one might expect to find small source dimensions and high stress drops. This could be exemplified by the selected aftershock data we investigated for the Imperial Valley, California, earthquake of 1940 (Trifunac, 1972b) and the San Fernando, California, earthquake of 1971 (Trifunac, 1972a; Trifunac, 1974).

As indicated by the trend of data in Figure 6, for larger earthquakes (larger M_L), a larger overall average stress could be released. However, the spread of the estimated stress-drop data for a given magnitude, M_L, appears to be about three orders of magnitude.

From the point of view of prediction of amplitudes of strong earthquake ground motion in earthquake engineering applications, it may not always be feasible to devise a simple method for estimating the possible stress drop for a given earthquake source. Consequently, at the present time, in virtually all estimations of the amplitudes of strong ground motion, the stress drop is overlooked and only one-parameter-scaling in terms of earthquake magnitude is being employed. Such simplification can be justified from the practical point of view, since the data and statistical analyses of earthquake magnitude are more complete and reliable than the interpretations of the inferred amplitudes of stress drop. For simplicity in presentation and in complying with the practical constraints in applications, in this paper we also use only the rough approximate theory which is based on one-parameter-scaling in terms of earthquake magnitude.

In the light of the above-mentioned simple assumptions and approximations, we feel that the stress estimates based on equations (4) and (13) and those derived from three independent source mechanism studies (Figures 6) are not in contradiction. However, due to the large scatter of stress drop data, it should be pointed out that the amplitudes of the peaks predicted by equation (4) could be uncertain by as much as a factor of about 2 to 3, even if one were to assume that the estimates of stress drop in Figure 6 and their scatter reflect the variability of stress drop rather than the uncertainties in the computations which are based on the approximate Brune's (1970) theory.

(*c*) *Peaks of strong-motion acceleration.* The largest apparent peak of strong-motion acceleration that might be recorded at the source of earthquake energy release ($R = 0$) seems to depend most prominently on the effective stress and the recording instrument employed to record it. The effective stress is believed to be proportional to the high-frequency amplitude of the Fourier transform of ground accelerations at the fault (Brune, 1970), while the recording instrument, which is usually a single-degree-of-freedom oscillator with damping close to 50 per cent of critical, represents a low-pass filter which attenuates frequencies higher than its natural frequency, ω_n, in a manner proportional to $(\omega/\omega_n)^2$. Many other parameters, no doubt, influence the largest amplitude of accelerations at the fault but will be neglected in this approximate analysis in which we only consider the simplest available model (Brune, 1970) which can readily be correlated with the apparent characteristics of the near-field and far-field observations.

The amplitude of the Fourier transform $F_{NF}(\omega)$, of particle accelerations at the fault surface can be shown to be approximately given by

$$\underset{\omega\to\infty}{F_{NF}(\omega)} = \frac{\sigma\beta}{\mu}\frac{\omega}{(\omega^2+\omega_\tau^2)^{\frac{1}{2}}} \tag{14}$$

(Brune, 1970), where $F_{NF}(\omega)$ is the Fourier transform of the absolute S-wave type accelerations, σ is the effective stress, β is the shear-wave velocity, and μ is the medium rigidity. For intermediate and low frequencies [$\omega \leqq \omega_\tau = 1/\tau$ and $\tau = \eta(r/\beta)$, where η is a numerical parameter whose values range from $\frac{1}{2}$ to 2 and r is the source dimension (Trifunac, 1973)], $F_{NF}(\omega)$ is proportional to $(\sigma\beta/\mu)\omega$.

It should be noted here that the constant high-frequency acceleration spectrum, $F_{NF}(\omega) = \sigma\beta/\mu$ when $\omega \gg \omega_\tau = 1/\tau$, results from a simple ramp in displacement, $d(t) = (\sigma\beta/\mu)t$, at the fault surface (Brune, 1970) and is caused by a Heaviside-type step in velocity at $t = 0$. This is clearly an oversimplification, since the nonlinear behavior of the fault gauge material must limit the accelerations to some finite values and this smooths out the discontinuity of the higher derivatives of $d(t)$ at $t = 0$. This smoothing operation acts as a low-pass filter on $F_{NF}(\omega)$ with the cut-off frequency say, ω_c. As an approximation it might be assumed that this filter is of the form $\omega_c^2/(\omega_c^2+\omega^2)$.

Unfortunately, there is no experimental evidence that comes from recorded strong-motion accelerograms at this time that could indicate what the realistic values of ω_c are for different types of geological materials at the fault. The closest strong-motion records available, so far, have been obtained at epicentral distances which are of the order of 10 km (Figure 1, 2 and 3) and in many cases the stations were not located on sound igneous rock. Consequently, the low values of Q for the high-frequency waves (say, $f >$ 20 Hz), geometric scattering, and possibly nonlinear response of shallow (less than 200 ft) soils, as well as the current digitization methods (Trifunac *et al.*, 1973), may all interfere with the high-frequency spectral amplitudes in a way that seems to eliminate any possibility of finding out what ω_c might be. On the other hand, several theoretical studies (e.g., Burridge and Willis, 1969; Kostrov, 1964; Richards, 1973) have demonstrated that when the rupture front arrives at a point on the fault the displacement may grow like part of a hyperbola. Such shearing deformations indicate then that the velocities and accelerations can be large in the vicinity of the rupture front; this suggests that ω_c may be quite large for faults that cut through sound igneous rock.

When recorded by a typical strong-motion accelerograph, the spectrum, $F_{NF}(\omega)$, is modified by the acceleration transfer function of the instrument whose amplitude, $H(\omega)$, is given by

$$H(\omega) = \left[\left(1-\frac{\omega^2}{\omega_n^2}\right)^2+\left(2\zeta\frac{\omega}{\omega_n}\right)^2\right]^{-\frac{1}{2}} \tag{15}$$

where ζ is the fraction of critical damping. For $\zeta \approx 0.50$, $H(\omega)$ can be approximated by

$$H^*(\omega) = \frac{\omega_0^2}{\omega_0^2+\omega^2} \tag{16}$$

where $\omega_0 \approx 2\omega_n$.

To compute the expected value of peak acceleration from the Fourier transform given by

$$F_{NF}(\omega) = \frac{\sigma\beta\omega_0^2}{\mu(\omega_0^2+\omega^2)}\frac{\omega_c^2}{(\omega_c^2+\omega^2)}\cdot\frac{\omega}{(\omega^2+\omega_\tau^2)^{\frac{1}{2}}} \tag{17}$$

we employ the method presented by Cartwright and Longuet-Higgins (1956) and the results of Udwadia and Trifunac (1974). According to this method, an estimate of the expected peak acceleration would be given by

$$E(a_{\max}) \approx m_0^{\frac{1}{2}} \sqrt{2}\{[\ln(1-\varepsilon^2)^{\frac{1}{2}}N]^{\frac{1}{2}} + \tfrac{1}{2}\gamma[\ln(1-\varepsilon^2)^{\frac{1}{2}}N]^{-\frac{1}{2}}\} \tag{18}$$

where m_0 is the zeroth moment of the power spectrum, $S_{NF}(\omega)$, of the near-field acceleration

$$m_0 = \int_0^\infty S_{NF}(\omega)\, d\omega \tag{19}$$

and $S_{NF}(\omega)$ can be approximated by

$$S_{NF}(\omega) \approx 1/T\,|F_{NF}(\omega)|^2 \tag{20}$$

where T is the duration of strong-motion shaking. In (18) ε represents a measure of power spectrum "width" and is approximately equal to 0.9 for $\zeta \approx 0.5$ and the spectrum $H^*(\omega)$ given by (16) (Udwadia and Trifunac, 1974). N is the total number of peaks of strong-motion acceleration in the time interval T and $\gamma = 0.5772$ is Euler's constant.

For typical strong shaking with duration of 25 sec, $N \approx 250$ and the factor $\{\cdot\}$ in (18) is approximately equal to 2.3 (Udwadia and Trifunac, 1974). The square root of the zeroth moment, $m_0^{\frac{1}{2}}$, then becomes

$$m_0^{\frac{1}{2}} \approx \left\{\frac{1}{T}\frac{\sigma^2\beta^2}{\mu^2}\int_0^\infty \frac{{\omega_0}^4}{({\omega_0}^2+\omega^2)^2}\cdot\frac{{\omega_c}^4}{({\omega_c}^2+\omega^2)^2}\cdot\frac{\omega^2\, d\omega}{(\omega^2+{\omega_\tau}^2)}\right\}^{\frac{1}{2}}$$

$$= \tfrac{1}{2}\left(\frac{\omega_0\pi}{T}\right)^{\frac{1}{2}}\frac{\sigma\beta}{\mu}\cdot R\left(\frac{\omega_\tau}{\omega_0}, \frac{\omega_0}{\omega_c}\right). \tag{21}$$

In (21), $R(\omega_\tau/\omega_0, \omega_0/\omega_c)$, which is always less than 1 (Figure 7), shows how nonzero ω_τ and finite ω_c reduce the amplitude of $m_0^{\frac{1}{2}}$. When ω_τ/ω_0 and ω_0/ω_c are small, $R(\omega_\tau/\omega_0, \omega_0/\omega_c)$ is close to 1.0, while for $\omega_\tau/\omega_0 = 0.2$ and $\omega_0/\omega_c = 4$ it reduces to about 0.3. For earthquakes studied in this paper ω_τ/ω_0 is always less than 0.1; if, on the basis of several theoretical solutions mentioned above (e.g., Burridge and Willis, 1969; Kostrov, 1964; Richards, 1973), we assume that ω_0/ω_c should be much less than one, then $R(\omega_\tau/\omega_0, \omega_0/\omega_c)$ is essentially equal to one and may be disregarded in the subsequent calculations which would then apply to reactivation of faults in otherwise sound igneous rock for earthquake magnitudes greater than say $M = 4$.

The natural frequency of a typical accelerograph is about 30 Hz. Typical values of the shear-wave velocity, β, and the rigidity, μ, are 3.0 km/sec and 1.0 to 3.0×10^{11} dynes/cm^2, respectively. For a stress drop (or effective stress) $\sigma = 1$ bar (10^6 dynes/cm^2) and $R(\omega_\tau/\omega_0, \omega_0/\omega_c) = 1$, one gets $m_0^{\frac{1}{2}} \approx 4$ to 10 cm/sec^2/bar; and for $N = 250$ and $\varepsilon = 0.9$, equation (18) then gives

$$E(a_{\max}) \approx 13-33 \text{ cm/sec}^2/\text{bar}. \tag{22}$$

Here we have assumed that $T = 25$ sec and $N = 250$. For $T = 10$, 5 and 2 sec and for the corresponding values of $N = 100$, 50 and 20, the expected value of $a_{\max}$/bar in (22) increases by factors equal to 1.4, 1.9 and 2.5, respectively.

Similar calculations have been carried out by Boore (1973) and Dietrich (1973). Boore, who normalized peak accelerations to effective stress, suggested that the peak acceleration could vary in a linear manner from about 25 cm/sec^2/bar, for a high-frequency cut-off equal to 10 Hz, to about 45 cm/sec^2/bar for a cut-off frequency equal to 20 Hz. In his

calculations, a low-pass filter with a cut-off frequency of 10 Hz approximately corresponds to the transfer function of an accelerograph with natural frequency of about 16 Hz and 60 per cent of critical damping. Figure 8 of Dietrich's paper, which presents parametrization of peak acceleration and distance by stress drop and minimum fault dimension for the cut-off frequency of about 10 Hz, suggests a range from about 30 cm/sec^2/bar to about 60 cm/sec^2/bar for peak accelerations at fault. In this paper we employ Brune's theory and the statistics of stationary random functions; Boore in his paper uses nonrandom approach and Brune's theory, while Dietrich employs deterministic finite element models which can have irregular frictional properties along the fault. In spite of the different methods and assumptions used, these three independent estimates of a_{max}/bar appear to be quite consistent.

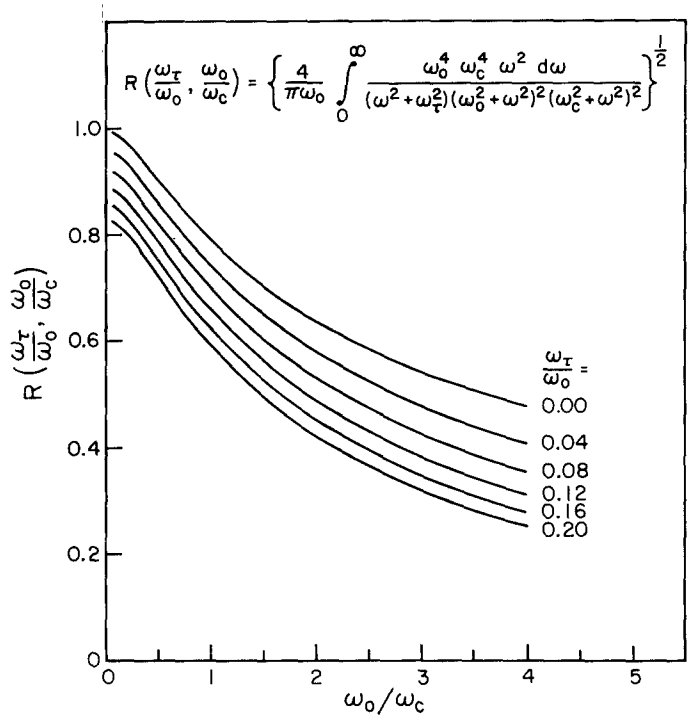

FIG. 7. $R(\omega_\tau/\omega_0, \omega_0/\omega_c)$ versus ω_0/ω_c and ω_τ/ω_0.

In view of the fact that the effective stress may vary from one point on the fault to another, it is not obvious whether a local maximum, local average, or an overall average of effective stress over the entire fault plane should be utilized to compute the expected amplitudes of peak acceleration in equation (22). The local stress maximum does not seem appropriate, since it may be associated with a wavelength too short to be of interest in the frequency band of earthquake engineering (0.05 to 30 Hz). The overall effective stress for a large earthquake could also be eliminated, since it would be associated with the wavelengths too long to contribute significantly to the peak accelerations which are influenced mostly by the amplitudes of intermediate and high-frequency points of the spectrum. We shall assume here, therefore, that the simple estimates of the effective stress which have been collected so far for intermediate and small earthquakes (Figure 6) could be considered as "representative" and in conjunction with equation (22) may be used for independent testing of the amplitudes summarized in Table 7. The perusal of the data in

Figure 6 shows that for $M_L \lesssim 6.5$ only a few of the estimates of stress drop in the Western United States exceed 100 bars. In fact, 90 per cent of all data in Figure 6 fall below about 140 bars, suggesting that the maximum peak accelerations associated with the approximate 90 per cent confidence level might range from about 2 g to about 5 g for the assumed duration of 25 sec. Considering the uncertainties in the foregoing assumptions, which are probably not worse than a factor of about 2 to 3, and the scatter of the computed data, the estimates of the maxima (Table 7) derived on the basis of equation (4) are obviously not contradicted by the estimates based on the simple source theory employed here.

It is interesting to note here that the peak amplitudes of the above maximum velocities and accelerations agree approximately with similar estimates derived by Ida (1973), whose calculations are based on a distinctly different physical basis. The Brune model is governed by the ambient tectonic stress, while Ida's analysis is based on the properties of medium which are related to the material strength against fracture.

Limitations of this Analysis and Possibilities for Future Improvements

Perhaps the most serious limitations of this analysis result from the insufficient number and nonuniformity of available data on peak amplitudes. This is so because most accelerograms come from the recording sites on alluvium (63 per cent) and from a narrow magnitude range between 6 and 7 (71 per cent). Furthermore, over 50 per cent of all data we used come from one earthquake, the San Fernando, California, earthquake of 1971. This may bias our present results, since this earthquake does not necessarily represent a typical shock from the source mechanism or from the instrumental coverage point of view.

Characterization of the amplitude attenuation with distance for peaks of acceleration, velocity, and displacement, which is better than the approximation based on $\log_{10} A_0(R)$, is clearly needed, especially at short distances which are less than about 20 km. In this respect one of the principal limitations of this paper may be related to the fact that we have neglected the dependence of the shape of the $\log_{10} A_0(R)$ curve on the source dimensions for small epicentral distances, where the radiation pattern and the proximity to the fault surface are likely to have a more well-defined effect on recorded amplitudes. When an adequate number of strong-motion data become available for all distances, especially for small epicentral distances, it will be possible to develop better amplitude attenuation laws which will depend on source size and the frequency band and amplitudes associated with the peak amplitudes. Although, as it has been pointed out in the above analysis, the empirical function $\log_{10} A_0(R)$ has several important characteristics which make it suitable for scaling of strong-motion data, it must be pointed out that it only represents our preliminary choice for an approximation of the amplitude attenuation law. Therefore, there must exist other attenuation laws which may describe this attenuation equally well or better than the $\log_{10} A_0(R)$ curve. .

Finally, the largest observed peaks of strong ground motion in the near-field will be determined by what can be transmitted through the materials directly beneath and surrounding the recording station. High-frequency high-acceleration pulses which in the linear range would lead to large forces will obviously be reduced by the nonlinear yielding response of the materials which have relatively lower strength.

The accuracy of the estimated dislocation amplitudes $\bar{u}$ in Figure 5, which have been calculated by using equation (11), is within a factor of about 3, which corresponds to 0.5 on the logarithmic scale used in this figure. The accuracy of magnitude determinations is about 0.3 magnitude units for the vertical scale in both Figures 5 and 6, while the estimates of stress drop in Figure 6 could be in error by as much as a factor of 3 to 5. Although

these errors increase the scatter of point estimates in Figures 5 and 6, in the foregoing analysis we assumed that the mean trend of the data is not affected.

We found that the formulas for peak amplitudes, when extrapolated from the available strong-motion data back to the source, at best do agree and at worst are not contradicted by the simple estimates of the corresponding quantities which are based on the source mechanism studies. However, these source mechanism studies have been derived on the basis of a simple source theory (Brune, 1970) which assumes instantaneous stress drop over the entire fault plane and consequently neglects the directional properties of the source (e.g., Ida and Aki, 1972). The Brune theory has been applied often to study the approximate estimates of the parameters which describe the source mechanism, and for many earthquakes the estimates of seismic moment, M_0, and source dimension, r, are now available. With the data from these studies, it now becomes possible to analyze the overall trends and distributions of such estimates and to examine the results from the viewpoint of strong earthquake ground motion. Other more realistic source mechanism models which are not based on the spontaneous stress drop over the whole fault plane require estimation of additional source parameters, e.g., velocity of rupture, and are inherently more complicated to analyze and/or require better data than what is currently available for most earthquakes. Therefore, only a small number of earthquakes in California have been studied by using three-dimensional moving dislocation models (e.g., Trifunac, 1974; Trifunac and Udwadia, 1974), and as yet there are not enough such studies to carry out a comparable statistical analysis as in Figure 5 or Figure 6.

In the formulation of the correlation functions (4) we have omitted source mechanism parameters like seismic moment, stress drop, or radiation pattern. This simplification clearly increases the uncertainty of our estimates, but it could be justified and has been motivated by the fact that in the majority of earthquake engineering characterizations of the potential source of earthquake energy release, typically, only magnitude is used to describe the size of an expected shock. Although source dimension and its orientation in space are often considered in some of the more advanced seismic risk analyses, this information is typically used only to compute the distance to the fault and not to calculate the radiation pattern or possible focusing effects that may result from a propagating rupture.

Conclusions

In this paper an attempt has been made to calculate approximate functional relationships that may exist between the different levels of peak acceleration, velocity, and displacement and such parameters as earthquake magnitude, epicentral distance, site conditions, and component direction. The coefficients employed in these relationships have been presented in a simple form which is convenient for applications. These coefficients represent our preliminary estimates, since the number of available strong-motion records is not adequate to derive the detailed description of the scaling laws involved.

The empirical attenuation curve for peak amplitudes of strong earthquake ground motion in Southern California can be approximated by the $\log_{10} A_0(R)$ curve proposed by Richter (1958) for scaling the peaks of instrumental response, which are used in the calculations of local magnitude, M_L. This can be demonstrated by direct comparison of this curve and the observed peaks for epicentral distances in the range from $R = 20$ to about $R = 200$ km. Although the amplitudes of $\log_{10} A_0(R)$ have been presented for epicentral distances less than 20 km (Richter, 1958), the lack of an adequate number of recorded strong-motion data for this distance range has not permitted evaluation of this

curve for short distances. To circumvent this lack of data, we computed the peak amplitudes for $R = 0$ by extrapolating the results based on epicentral distances greater than 20 km back to the source and assumed that the $\log_{10} A_0(R)$ curve applies there as well. We then compared the resulting peak amplitudes with independent estimates of peak acceleration, velocity, and displacement which could be derived from three studies dealing with source mechanism of earthquakes in Southern California (Trifunac, 1972a, 1972b; Thatcher and Hanks, 1973) and found that there is no apparent contradiction between these two independent calculations.

The approximately parabolic growth of the functions $\log_{10} [a_0(M, p, s, v)]$, $\log_{10} [v_0(M, p, s, v)]$, and $\log_{10} [d_0(M, p, s, v)]$ with magnitude approaches the slope equal to 1 for magnitudes equal to 5 to 6.5. This means that the logarithms of the peak amplitudes of strong ground motion do not grow linearly with magnitude and that this rate of growth becomes very small for magnitudes greater than 6.5 to 7.0. For a magnitude 7.5 shock the peaks of the near-field strong ground motion seem to reach the maximum amplitudes. For magnitude $M = 7.5$, 90 per cent confidence level, and epicentral distance $R = 0$, the estimated maximum amplitudes of strong-motion acceleration, velocity, and displacement are approximately equal to 3 to 5 g, 400 to 700 cm/sec, and 200 to 400 cm, respectively. According to this analysis, these amplitudes would be associated with the largest earthquakes in the Western United States.

The effect of geological site conditions on the confidence levels of peak accelerations has been found to be insignificant. The confidence levels for amplitudes of peak velocities and peak displacements are about 90 per cent and 250 per cent higher on alluvium ($s = 0$) sites when compared with the corresponding level for basement rock sites ($s = 2$).

We found that the amplitudes of strong ground motion in the near-field of earthquake energy release appear to be higher than so far predicted by some previous investigators (e.g., Gutenberg and Richter, 1956; Housner, 1965; Blume, 1965; Milne and Davenport, 1969; Esteva, 1970). These differences can be explained by the serious lack of near-field data ($R < 20$ km) and by the use of somewhat arbitrary methods for extrapolation toward the earthquake source in several previous studies. In this respect, this paper suffers from a similar difficulty associated with the lack of recorded accelerograms for epicentral distances less than about 20 km. However, our use of the $\log_{10} A_0(R)$ function for extrapolating back to the source offers the advantage that the predicted amplitudes of acceleration, velocity, and displacement at $R = 0$ which are based on $\log_{10} A_0(R = 0)$ seem not to be contradicted (within a factor of about 2 to 3) by the amplitudes calculated from other independent source mechanism studies for the representative earthquakes and the same geographic area where most of the strong-motion data which are used in this paper have been recorded. Therefore, while we do expect that our scaling functions and parameters will have to be improved and updated as the data bank becomes more abundant and representative, there seems to be no reason to expect that these changes will be as large as differences between the amplitudes presented in this paper and in several previous studies.

Finally, it should be pointed out here that, from the practical earthquake engineering point of view, high acceleration amplitudes should not necessarily be associated with a proportionally higher destructive potential. An extended duration of strong ground motion and high acceleration amplitudes characterize destructive earthquake shaking, while one or several high-frequency high-acceleration peaks may, in fact, constitute only minor excitation because of the short duration involved and may lead to only moderate or small impulses when applied to a structural system.

Acknowledgments

I thank K. Aki, A. G. Brady, J. N. Brune, T. C. Hanks, G. W. Housner, D. E. Hudson, and P. G. Richards for critical reading of the manuscript and for useful discussions. I am especially indebted to D. M. Boore and J. E. Luco whose comments and critical suggestions led to several important additions and improvements of this paper.

This research has been supported in part by the Earthquake Research Affiliates Program at the California Institute of Technology and by the United States Geological Survey.

References

Blume, J. A. (1965). Earthquake ground motion and engineering procedures for important installations near active faults, *Proc. World Conf. Earthquake Eng., 3rd, New Zealand* **4**, 53–67.

Boore, D. M. (1973). Empirical and theoretical study of near-fault wave propagation, *Proc. World Conf. Earthquake Eng., 5th, Rome*, Italy.

Brune, J. N. (1970). Tectonic stress and the spectra of seismic shear waves from earthquakes, *J. Geophys. Res.* **75**, 4997–5009.

Burridge, R. and J. Willis (1969). The self similar problem of the expanding elliptical crack in an anisotropic solid, *Proc. Cambridge Phil. Soc.* **66**, 439–468.

Cartwright, D. E. and M. S. Longuet-Higgins (1956). The statistical distribution of maxima of a random function, *Proc. Roy. Soc. London, Ser. A* **237**, 212–232.

Cloud, W. K. and V. Perez (1971). Unusual accelerograms recorded at Lima, Peru, *Bull. Seism. Soc. Am.* **61**, 633–640.

Dietrich, J. H. (1973). A deterministic near-field source model, *Proc. World Conf. Earthquake Eng., 5th, Rome*, Italy.

Donovan, N. C. (1972). Earthquake hazards for buildings, in *Building Practices for Disaster Mitigation*, National Bureau of Standards Building Science Series 46, Boulder, Colorado.

Esteva, L. (1970). Seismic risk and seismic design decisions in *Seismic Design for Nuclear Power Plants*, R. J. Hansen, Editor, Mass. Inst. Tech. Press, Cambridge, Mass.

Gutenberg, B. and C. F. Richter (1942). Earthquake magnitude, intensity, energy and acceleration, *Bull. Seism. Soc. Am.*, **32**, 163–191.

Gutenberg, B. and C. F. Richter (1956). Earthquake magnitude, intensity, energy and acceleration, II, *Bull. Seism. Soc. Am.* **46**, 105–195.

Hanks, T. C. and M. Wyss (1972). The use of body-wave spectra in the determination of seismic source parameters, *Bull. Seism. Soc. Am.* **62**, 561–590.

Haskell, N. A. (1969). Elastic displacements in the near-field of a propagating fault, *Bull. Seism. Soc. Am.* **59**, 865–908.

Housner, G. W. (1965). Intensity of earthquake ground shaking near the causative fault, *Proc. World Conf. Earthquake Eng., 3rd, New Zealand*, 94–111.

Hudson, D. E., A. G. Brady, M. D. Trifunac, and A. Vijayaraghavan (1971). Strong-motion earthquake accelerograms, corrected accelerograms and integrated velocity and displacement curves, Vol. II, Part A, Earthquake Eng. Res. Lab., *EERL 71–51*, Calif. Inst. of Tech., Pasadena, California.

Ida, Y. (1973). The maximum acceleration of seismic ground motion, *Bull. Seism. Soc. Am.* **63**, 959–968.

Ida, Y. and K. Adi (1972). Seismic source time function of propagating longitudinal-shear cracks, *J. Geophys. Res.* **77**, 2034–2044.

Kanai, K. (1966). Improved empirical formula for characteristics of stray earthquake motions, *Proc. Japan. Earthquake Symp.*, 1–4 (in Japanese).

Katayama, T. (1974). Statistical analysis of peak accelerations of recorded earthquake ground motions, Seisan Kenkyu, *J. Inst. Ind. Sci., Univ. of Tokyo* **26**, 18–20.

Kostrov, B. V. (1964). Selfsimilar problems of propagation of shear cracks, *J. Appl. Math. Mech.* **28**, 1077–1087.

Milne, W. G. and A. G. Davenport (1969). Distribution of earthquake risk in Canada, *Bull. Seism. Soc. Am.* **59**, 754–779.

Neumann, F. (1954). *Earthquake Intensity and Related Ground Motion*, Univ. of Washington Press, Seattle, Washington.

Nuttli, O. W. (1973). Seismic wave attenuation and magnitude relations for Eastern North America, *J. Geophys. Res.* **78**, 876–885.

Page, R. A., D. M. Boore, W. B. Joyner, and H. W. Coulter (1972). Ground Motion Values for Use in the Seismic Design of the Trans-Alaska Pipeline System, *Geological Survey Circular 672*, Washington, D.C.

Richards, P. G. (1973). The dynamic field of a growing plane elliptical shear crack, *J. Solids Structure* **9**, 843–861.

Richter, C. F. (1958). *Elementary Seismology*, Freeman, San Francisco.

Schnabel, P. and H. B. Seed (1973). Accelerations in rock for earthquakes in the Western United States, *Bull. Seism. Soc. Am.* **63**, 501–516.

Thatcher, W. and T. C. Hanks (1973). Source parameters of Southern California earthquakes, *J. Geophys. Res.* **78**, 8547–8576.

Trifunac, M. D. (1971). Surface motion of a semi-cylindrical alluvial valley for incident plane *SH* waves, *Bull. Seism. Soc. Am.* **61**, 1739–1753.

Trifunac, M. D. (1971). Zero baseline correction of strong-motion accelerograms, *Bull. Seism. Soc. Am.* **61**, 1201–1211.

Trifunac, M. D. (1972a). Stress estimates for San Fernando, California, earthquake of February 9, 1971: Main event and thirteen aftershocks, *Bull. Seism. Soc. Am.* **62**, 721–750.

Trifunac, M. D. (1972b). Tectonic stress and source mechanism of the Imperial Valley, California, earthquake of 1940, *Bull. Seism. Soc. Am.* **62**, 1283–1302.

Trifunac, M. D. (1972c). A note on correction of strong-motion accelerograms for instrument response, *Bull. Seism. Soc. Am.* **62**, 401–409.

Trifunac, M. D. (1973). Analysis of strong earthquake ground motion for prediction of response spectra, *Intern. J. Earthquake Eng. Struct. Dyn.* **2**, 59–69.

Trifunac, M. D. (1974). A three-dimensional dislocation model for the San Fernando, California, earthquake of February 9, 1971, *Bull. Seism. Soc. Am.* **64**, 149–172.

Trifunac, M. D. and V. E. Lee (1973). Routine Computer Processing of Strong-Motion Accelerograms, Earthquake Eng. Res. Lab., *EERL 73-03*, Calif. Inst. of Tech., Pasadena, Calif.

Trifunac, M. D. and V. E. Lee (1974). A note on the accuracy of computed ground displacements from strong-motion accelerograms, *Bull. Seism. Soc. Am.* **64**, 1209–1219.

Trifunac, M. D. and A. G. Brady (1975a). On the correlation of seismic intensity scales with the peaks of recorded strong ground motion, *Bull. Seism. Soc. Am.* **65**, 139–162.

Trifunac, M. D. and A. G. Brady (1975b). Correlations of peak acceleration, velocity and displacement with earthquake magnitude, distance and site conditions, *Intern. J. Earthquake Eng. and Dyn. Struct.* (in press).

Trifunac, M. D. and A. G. Brady (1975c). A study on the duration of strong earthquake ground motion, *Bull. Seism. Soc. Am.* **65**, 581–626.

Trifunac, M. D. and F. E. Udwadia (1974). Parkfield, California, earthquake of June 27, 1966: A three-dimensional moving dislocation, *Bull. Seism. Soc. Am.* **64**, 511–533.

Trifunac, M. D., F. E. Udwadia, and A. G. Brady (1973). Analysis of errors in digitized strong-motion accelerograms, *Bull. Seism. Soc. Am.* **63**, 157–187.

Udwadia, F. E. and M. D. Trifunac (1974). Characterization of response spectra through the statistics of oscillator response, *Bull. Seism. Soc. Am.* **64**, 205–219.

Wong, H. L. and M. D. Trifunac (1974). Surface motion of a semi-elliptical alluvial valley for incident plane *SH* waves, *Bull. Seism. Soc. Am.* **64**, 1289–1403.

EARTHQUAKE ENGINEERING RESEARCH LABORATORY
CALIFORNIA INSTITUTE OF TECHNOLOGY
PASADENA, CALIFORNIA 91125

Manuscript received March 17, 1975